

Investigation of two *Fermi*-LAT gamma-ray blazars coincident with high-energy neutrinos detected by IceCube

***Fermi*-LAT collaboration:** S. Garrappa⁶¹, S. Buson^{57, 58, 59}, A. Franckowiak⁶¹

ASAS-SN: B. J. Shappee³⁰, J. F. Beacom^{20, 19, 21}, S. Dong⁸, T. W.-S. Holoien⁴⁷, C. S. Kochanek^{19, 21}, J. L. Prieto^{48, 49}, K. Z. Stanek¹⁹, T. A. Thompson¹⁹

IceCube collaboration: M. G. Aartsen¹⁷, M. Ackermann⁶¹, J. Adams¹⁷, J. A. Aguilar¹³, M. Ahlers²², M. Ahrens⁵⁰, C. Alispach²⁸, D. Altmann²⁶, K. Andeen³⁸, T. Anderson⁵⁵, I. Ansseau¹³, G. Anton²⁶, C. Argüelles¹⁵, J. Auffenberg¹, S. Axani¹⁵, P. Backes¹, H. Bagherpour¹⁷, X. Bai⁴⁴, A. Barbano²⁸, S. W. Barwick³¹, V. Baum³⁷, R. Bay⁹, J. J. Beatty^{20, 19}, K.-H. Becker⁶⁰, J. Becker Tjus¹², S. BenZvi⁴⁶, D. Berley¹⁸, E. Bernardini⁶¹, D. Z. Besson³², G. Binder^{10, 9}, D. Bindig⁶⁰, E. Blaufuss¹⁸, S. Blot⁶¹, C. Boehm⁵⁰, M. Börner²³, S. Böser³⁷, O. Botner⁵⁶, E. Bourbeau²², J. Bourbeau³⁶, F. Bradascio⁶¹, J. Braun³⁶, H.-P. Bretz⁶¹, S. Bron²⁸, J. Brostean-Kaiser⁶¹, A. Burgman⁵⁶, R. S. Busse³⁶, T. Carver²⁸, C. Chen⁶, E. Cheung¹⁸, D. Chirkin³⁶, K. Clark³³, L. Classen³⁹, G. H. Collin¹⁵, J. M. Conrad¹⁵, P. Coppin¹⁴, P. Correa¹⁴, D. F. Cowen^{55, 54}, R. Cross⁴⁶, P. Dave⁶, J. P. A. M. de André²⁴, C. De Clercq¹⁴, J. J. DeLaunay⁵⁵, H. Dembinski⁴⁰, K. Deoskar⁵⁰, S. De Ridder²⁹, P. Desiati³⁶, K. D. de Vries¹⁴, G. de Wasseige¹⁴, M. de With¹¹, T. DeYoung²⁴, J. C. Díaz-Vélez³⁶, H. Dujmovic⁵², M. Dunkman⁵⁵, E. Dvorak⁴⁴, B. Eberhardt³⁶, T. Ehrhardt³⁷, P. Eller⁵⁵, P. A. Evenson⁴⁰, S. Fahey³⁶, A. R. Fazely⁷, J. Felde¹⁸, K. Filimonov⁹, C. Finley⁵⁰, A. Franckowiak⁶¹, E. Friedman¹⁸, A. Fritz³⁷, T. K. Gaisser⁴⁰, J. Gallagher³⁵, E. Ganster¹, S. Garrappa⁶¹, L. Gerhardt¹⁰, K. Ghorbani³⁶, T. Glauch²⁷, T. Glüsenskamp²⁶, A. Goldschmidt¹⁰, J. G. Gonzalez⁴⁰, D. Grant²⁴, Z. Griffith³⁶, M. Gündüz¹², C. Haack¹, A. Hallgren⁵⁶, L. Halve¹, F. Halzen³⁶, K. Hanson³⁶, D. Hebecker¹¹, D. Heereman¹³, K. Helbing⁶⁰, R. Hellauer¹⁸, F. Henningsen²⁷, S. Hickford⁶⁰, J. Hignight²⁴, G. C. Hill², K. D. Hoffman¹⁸, R. Hoffmann⁶⁰, T. Hoinka²³, B. Hokanson-Fasig³⁶, K. Hoshina^{36, 62}, F. Huang⁵⁵, M. Huber²⁷, K. Hultqvist⁵⁰, M. Hünnefeld²³, R. Hussain³⁶, S. In⁵², N. Iovine¹³, A. Ishihara¹⁶, E. Jacobi⁶¹, G. S. Japaridze⁵, M. Jeong⁵², K. Jero³⁶, B. J. P. Jones⁴, P. Kalaczynski¹, W. Kang⁵², A. Kappes³⁹, D. Kappesser³⁷, T. Karg⁶¹, M. Karl²⁷, A. Karle³⁶, U. Katz²⁶, M. Kauer³⁶, A. Keivani⁵⁵, J. L. Kelley³⁶, A. Kheirandish³⁶, J. Kim⁵², T. Kintscher⁶¹, J. Kiryluk⁵¹, T. Kittler²⁶, S. R. Klein^{10, 9}, R. Koirala⁴⁰, H. Kolanoski¹¹, L. Köpke³⁷, C. Kopper²⁴, S. Kopper⁵³, D. J. Koskinen²², M. Kowalski^{11, 61}, K. Krings²⁷, G. Krückl³⁷, N. Kulacz²⁵, S. Kunwar⁶¹, N. Kurahashi⁴³, A. Kyriacou², M. Labare²⁹, J. L. Lanfranchi⁵⁵, M. J. Larson¹⁸, F. Lauber⁶⁰, J. P. Lazar³⁶, K. Leonard³⁶, M. Leuermann¹, Q. R. Liu³⁶, E. Lohfink³⁷, C. J. Lozano Mariscal³⁹, L. Lu¹⁶, F. Lucarelli²⁸, J. Lünemann¹⁴, W. Luszczak³⁶, J. Madsen⁴⁵, G. Maggi¹⁴, K. B. M. Mahn²⁴, Y. Makino¹⁶, K. Mallot³⁶, S. Mancina³⁶, I. C. Mariş¹³, R. Maruyama⁴¹, K. Mase¹⁶, R. Maunu¹⁸, K. Meagher³⁶, M. Medici²², A. Medina²⁰, M. Meier²³, S. Meighen-Berger²⁷, T. Menne²³, G. Merino³⁶, T. Meures¹³, S. Miarecki^{10, 9}, J. Micallef²⁴, G. Momenté³⁷, T. Montaruli²⁸, R. W. Moore²⁵, M. Moulai¹⁵, R. Nagai¹⁶, R. Nahnauer⁶¹, P. Nakarmi⁵³, U. Naumann⁶⁰, G. Neer²⁴, H. Niederhausen²⁷, S. C. Nowicki²⁵, D. R. Nygren¹⁰, A. Obertacke Pollmann⁶⁰, A. Olivas¹⁸, A. O'Murchadha¹³, E. O'Sullivan⁵⁰, T. Palczewski^{10, 9}, H. Pandya⁴⁰, D. V. Pankova⁵⁵, N. Park³⁶, P. Peiffer³⁷, C. Pérez de los Heros⁵⁶, D. Pieloth²³, E. Pinat¹³, A. Pizzuto³⁶, M. Plum³⁸, P. B. Price⁹, G. T. Przybylski¹⁰, C. Raab¹³, A. Raissi¹⁷, M. Rameez²², L. Rauch⁶¹, K. Rawlins³, I. C. Rea²⁷, R. Reimann¹, B. Relethford⁴³, G. Renzi¹³, E. Resconi²⁷, W. Rhode²³, M. Richman⁴³, S. Robertson¹⁰, M. Rongen¹, C. Rott⁵², T. Ruhe²³, D. Ryckbosch²⁹, D. Rysewyk²⁴, I. Safa³⁶, S. E. Sanchez Herrera²⁵, A. Sandrock²³, J. Sandroos³⁷, M. Santander⁵³, S. Sarkar⁴², S. Sarkar²⁵, K. Satalecka⁶¹, M. Schaufel¹, P. Schlunder²³, T. Schmidt¹⁸, A. Schneider³⁶, J. Schneider²⁶, L. Schumacher¹, S. Sclafani⁴³, D. Seckel⁴⁰, S. Seunarine⁴⁵, M. Silva³⁶, R. Snihur³⁶, J. Soedingrekso²³, D. Soldin⁴⁰, M. Song¹⁸, G. M. Spiczak⁴⁵, C. Spiering⁶¹, J. Stachurska⁶¹, M. Stamatikos²⁰, T. Stanev⁴⁰, A. Stasik⁶¹, R. Stein⁶¹, J. Stettner¹, A. Steuer³⁷, T. Stezelberger¹⁰, R. G. Stokstad¹⁰, A. Stöhl¹⁶, N. L. Strotjohann⁶¹, T. Stuttard²², G. W. Sullivan¹⁸, M. Sutherland²⁰, I. Taboada⁶, F. Tenholt¹², S. Ter-Antonyan⁷, A. Terliuk⁶¹, S. Tilav⁴⁰, L. Tomankova¹², C. Tönnis⁵², S. Toscano¹⁴, D. Tosi³⁶, M. Tselengidou²⁶, C. F. Tung⁶, A. Turcati²⁷, R. Turcotte¹, C. F. Turley⁵⁵, B. Ty³⁶, E. Unger⁵⁶, M. A. Unland Elorrieta³⁹, M. Usner⁶¹, J. Vandenbroucke³⁶, W. Van Driessche²⁹, D. van Eijk³⁶, N. van Eijndhoven¹⁴, S. Vanheule²⁹, J. van Santen⁶¹, M. Vraeghe²⁹, C. Walck⁵⁰, A. Wallace², M. Wallraff¹, N. Wandkowsky³⁶, T. B. Watson⁴, C. Weaver²⁵, M. J. Weiss⁵⁵, J. Weldert³⁷, C. Wendt³⁶, J. Werthebach³⁶, S. Westerhoff³⁶, B. J. Whelan², N. Whitehorn³⁴, K. Wiebe³⁷, C. H. Wiebusch¹, L. Wille³⁶, D. R. Williams⁵³, L. Wills⁴³, M. Wolf²⁷, J. Wood³⁶, T. R. Wood²⁵, K. Woschnagg⁹, G. Wrede²⁶, D. L. Xu³⁶, X. W. Xu⁷, Y. Xu⁵¹, J. P. Yanez²⁵, G. Yodh³¹, S. Yoshida¹⁶, T. Yuan³⁶

(Affiliations can be found after the references)

June 11, 2022

Send offprint requests to: simone.garrappa@desy.de

ABSTRACT

Gamma-ray blazars have been suggested as promising contributors to the diffuse flux of high-energy neutrinos detected by IceCube. After the identification of the gamma-ray blazar TXS 0506+056 as the first compelling IceCube neutrino source candidate, a systematic analysis of all high-energy neutrino events satisfying the IceCube realtime trigger criteria was performed. One additional known gamma-ray source, the blazar GB6 J1040+0617, was found to be in spatial coincidence with a neutrino in this sample. The chance probability of this coincidence is 30% after trials correction. For the first time, we present a systematic study of the gamma-ray flux, spectral and optical variability and multi-wavelength behavior of GB6 J1040+0617 and compare it to TXS 0506+056. We discuss a possible source confusion with a new emerging gamma-ray source, the blazar 4C+06.41. We find that TXS 0506+056 shows strong flux variability in the *Fermi*-LAT gamma-ray band, being in an active state around the arrival of IceCube-170922A, but in a low state during the archival IceCube neutrino flare in 2014/15. In both cases the spectral shape is statistically compatible ($\leq 2\sigma$) with the average spectrum.

Assuming the reported redshift estimate of $z=0.73$, GB6 J1040+0617 has an average gamma-ray luminosity comparable with that of TXS 0506+056. It shows a bright optical flare recorded by ASAS-SN accompanied by modest gamma-ray activity at the neutrino arrival time. While the association with the neutrino is consistent with background expectations, GB6 J1040+0617 appears to be a plausible neutrino source candidate based on its energetics and multi-wavelength features. Finding one or two neutrinos originating from gamma-ray blazars in the given sample of high-energy neutrinos is consistent with previously derived limits of neutrino emission from gamma-ray blazars, indicating the sources of the majority of cosmic high-energy neutrinos remains unknown.

Key words. astroparticle physics — neutrinos — Galaxies: active — BL Lacertae objects: individual:TXS 0506+056, GB6 J1040+0617, 4C+06.41, SDSS J104039.54+061521.5

1. Introduction

The IceCube Neutrino Observatory has detected a diffuse flux of high-energy neutrinos (Aartsen et al. 2015, 2013). However, until recently no compelling evidence for spatial or temporal clustering of events had been identified and the origin of the neutrinos was unknown (Aartsen et al. 2017a; Aartsen et al. 2015). The arrival directions of IceCube neutrinos are compatible with an isotropic distribution, suggesting a predominant extra-galactic origin of the cosmic neutrinos. Among the most promising source candidates are (low luminosity) gamma-ray bursts, choked-jet and interacting supernovae, tidal disruption events, star forming galaxies and active galactic nuclei (AGN) - see Ahlers & Halzen (2015) for a recent review. In general, high-energy neutrinos are produced through interactions of cosmic rays with ambient matter or photon fields. Charged and neutral pions produced in those interactions produce neutrinos and gamma rays, respectively, in their decay chain.

Blazars, those AGN with a relativistic jet of plasma pointing towards the observer, have been suggested as high-energy cosmic-ray accelerators and, in turn, neutrino sources (e.g. Mannheim 1995; Stecker 2013; Padovani & Resconi 2014; Murase 2015; Tavecchio & Ghisellini 2015; Kadler et al. 2016; Krauß et al. 2016). In their jets, protons (as well as electrons) might be accelerated and interact with lower-energy photons (e.g. produced by the accretion disk or other external fields) and produce neutrinos and gamma rays.

The spectral energy distribution (SED) of blazars exhibits two broad bumps. While the lower-energy one is thought to arise from synchrotron radiation of primary electrons, the origin of the higher-energy one is still a matter of debate. Both leptonic and hadronic models are capable of adequately reproducing the observed emission for most sources.

Hints of correlation between neutrinos and blazar positions have been suggested by several groups (e.g. Kadler et al. 2016; Padovani et al. 2016; Krauß et al. 2016; Lucarelli et al. 2019). It is evident that multi-messenger studies are crucial to probe various source classes as potential neutrino emitters (Bartos & Kowalski 2017), as well as shed light onto the emission mechanisms of blazars.

To enable an efficient search for transient electromagnetic counterparts to the high-energy astrophysical neutrino signal, IceCube has implemented a realtime program (Aartsen et al. 2017b). The program selects high-energy neutrinos of likely cosmic origin within seconds of their detection at the South Pole, and distributes the information of the reconstructed neutrino direction to a network of follow-up instruments. On September 22, 2017, the program released an alert reporting a well-reconstructed >100 TeV event, IceCube-170922A. Shortly after, the *Fermi* Large Area Telescope (LAT) collaboration reported the detection of a potential electromagnetic counterpart in spatial coincidence with this high-energy neutrino event (Tanaka et al. 2017). The gamma-ray signal was consistent with the known gamma-ray blazar, TXS 0506+056, which at the time of the IceCube trigger was in a state of enhanced activity (Aartsen et al. 2018a). Subsequently, >100 GeV gamma-ray emission was detected from TXS 0506+056 for the first time by the Major Atmospheric Gamma Imaging Cherenkov Telescopes (MAGIC, Aartsen et al. 2018a; Ansoldi et al. 2018), which was later confirmed by the Very Energetic Radiation Imaging Telescope Array System (VERITAS, Abeysekara et al. 2018). Searches with the ANTARES neutrino telescope yielded no convincing evidence of additional neutrino emission related to the source (Albert et al. 2018).

The chance probability for a neutrino detection in spatial coincidence with the flaring blazar was estimated to 3σ (Aartsen et al. 2018a). An archival search for additional >100 GeV neutrinos from the location of TXS 0506+056

led to the discovery of a candidate neutrino flare between September 2014 and March 2015 at 3.5σ significance (Aartsen et al. 2018b). The possible detection of neutrino emission from the blazar has motivated several attempts to model the multi-wavelength spectral energy distribution of TXS 0506+056, assuming simultaneous leptonic and hadronic emission in so-called hybrid models (see e.g. Gao et al. 2018; Ansoldi et al. 2018; Cerruti et al. 2019; Keivani et al. 2018).

A second spatial coincidence was pointed out in Aartsen et al. (2018a) of an archival high-energy neutrino event with the *Fermi* source 3FGL J1040.4+0615.

In this paper we carry out a study of potential *Fermi* gamma-ray counterparts to the high-energy events observed by IceCube. Presented is a detailed investigation of the candidate electromagnetic counterparts found in spatial connection to two high-energy IceCube neutrino alerts.

2. Search for high-energy neutrinos in coincidence with gamma-ray sources

The IceCube neutrino observatory is a cubic kilometer scale Cherenkov detector located at a depth of 1450 m to 2450 m in the clear ice of the geographic South Pole. A total of 5160 digital optical modules are located on 86 strings arranged in a hexagonal grid to detect Cherenkov light emitted by secondary charged particles produced in neutrino interactions in or close to the instrumented detector volume (Aartsen et al. 2017a).

The sample of neutrinos considered in this study is based on the high-energy neutrino events observed by the IceCube detector from 2010 to 2017, and satisfying the IceCube realtime trigger criteria. This includes ten published realtime alerts (up to and including IceCube-170922A) and forty archival events¹. Among the latter, five are flagged because of their poor angular reconstruction, which would have caused them to be retracted as realtime alerts. To reduce the number of chance coincidences, we apply the same sample selection cut of Aartsen et al. (2018a) and restrict the study to events with a 90% angular uncertainty² smaller than 5° . Eight events do not satisfy this criteria and are thus discarded. The final neutrino sample consists of thirty seven well-reconstructed events. Each event is cross checked with the Third *Fermi*-LAT Point Source Catalog (3FGL, Acero et al. 2015) and the Third *Fermi*-LAT Catalog of High-Energy Sources (3FHL, Ajello et al. 2017) to search for spatial coincidences with known gamma-ray sources.

Among the remaining 37 neutrino events, besides the IceCube-170922A/TXS 0506+056 occurrence, one additional spatial coincidence with a gamma-ray source is confirmed in this search. The gamma-ray source 3FGL J1040.4+0615 (Ackermann et al. 2015), which is associated with GB6 J1040+0617, a BL Lac object with redshift 0.7351 ± 0.0045 (Maselli et al. 2015; Ahn et al. 2012)³, is lo-

cated within the 90% uncertainty of the well-reconstructed neutrino IceCube-141209A.

We focus on the potential astrophysical counterparts of these two high-energy neutrinos, and present a detailed investigation of the gamma-ray properties enabled by the continuous all-sky coverage of the *Fermi*-LAT.

3. *Fermi*-LAT data

The *Fermi*-LAT is a pair-conversion telescope sensitive to gamma rays with energies from 20 MeV to greater than 300 GeV (Atwood et al. 2009). It has a large field of view and scans the entire sky every three hours during standard operation, making it well suited to monitor variable gamma-ray sources on different timescales, from seconds to years.

In this study we use 9.6 years of Pass 8 *Fermi*-LAT data collected between 2008 August 4 and 2018 March 16 (MJD 54682-58193) selecting photons from the event class developed for point source analyses⁴. We perform a likelihood analysis, binned in space and energy, using the standard *Fermi*-LAT ScienceTools package version v11r5p3 available from the *Fermi* Science Support Center⁵ (FSSC) and the P8R2_SOURCE_V6 instrument response functions, together with the *fermipy* package v0.16.0. We analyse data in the energy range of 100 MeV to 1 TeV binned into eight logarithmically-spaced energy intervals per decade. To minimize the contamination from gamma rays produced in the Earth's upper atmosphere, we apply an instrument zenith angle cut of $\theta < 90^\circ$. We remove time periods coinciding with solar flares and gamma-ray bursts detected by the LAT. The effect of energy dispersion is included in the fits performed with the *Fermi*-LAT ScienceTools.

In the analysis of GB6 J1040+0617, an additional data cut is applied to remove the time periods when the Sun was located less than 15° from the source position. This additional cut is necessary because the position of GB6 J1040+0617 lies very close to the ecliptic.

For each source, we select a $10^\circ \times 10^\circ$ region of interest (ROI) centered on the source position, binned in 0.1 size pixels. The binning is applied in celestial coordinates using an Aitoff projection. The input model for the ROI includes all known gamma-ray sources from the 3FGL catalog in a region of $15^\circ \times 15^\circ$, slightly larger than the ROI, and the isotropic and Galactic diffuse gamma-ray emission models provided by the standard templates `iso_P8R2_SOURCE_V6_v06.txt` (extrapolated linearly in the logarithm up to 1 TeV) and `gll_iem_v06.fits`⁶.

Given the different and longer integration time of our analysis with respect to the 3FGL, we search for new gamma-ray sources that were too faint for being included in the 3FGL. New putative point sources are modeled with a single power law spectrum, with index fixed to 2 and normalisation free to vary in the fit. The search procedure is iterated until no further significant ($TS_{dec} > 25$) excess is found. The new point sources significantly detected in the longer-integration time dataset are accounted for by the final ROI model.

¹ https://icecube.wisc.edu/science/data/TXS0506_alerts

² We note that the uncertainty contours considered here are a result of the processing techniques applied at the time and may experience small changes with future analysis improvements that reflect more accurate treatment of the systematic uncertainties.

³ We note that the redshift measurement might be unreliable given that the automatic extraction was flagged by the SDSS pipeline, which indicates a poorly determined redshift.

⁴ http://fermi.gsfc.nasa.gov/ssc/data/analysis/documentation/Pass8_usage.html

⁵ <http://fermi.gsfc.nasa.gov/ssc/data/analysis/>

⁶ <https://fermi.gsfc.nasa.gov/ssc/data/access/lat/BackgroundModels.html>

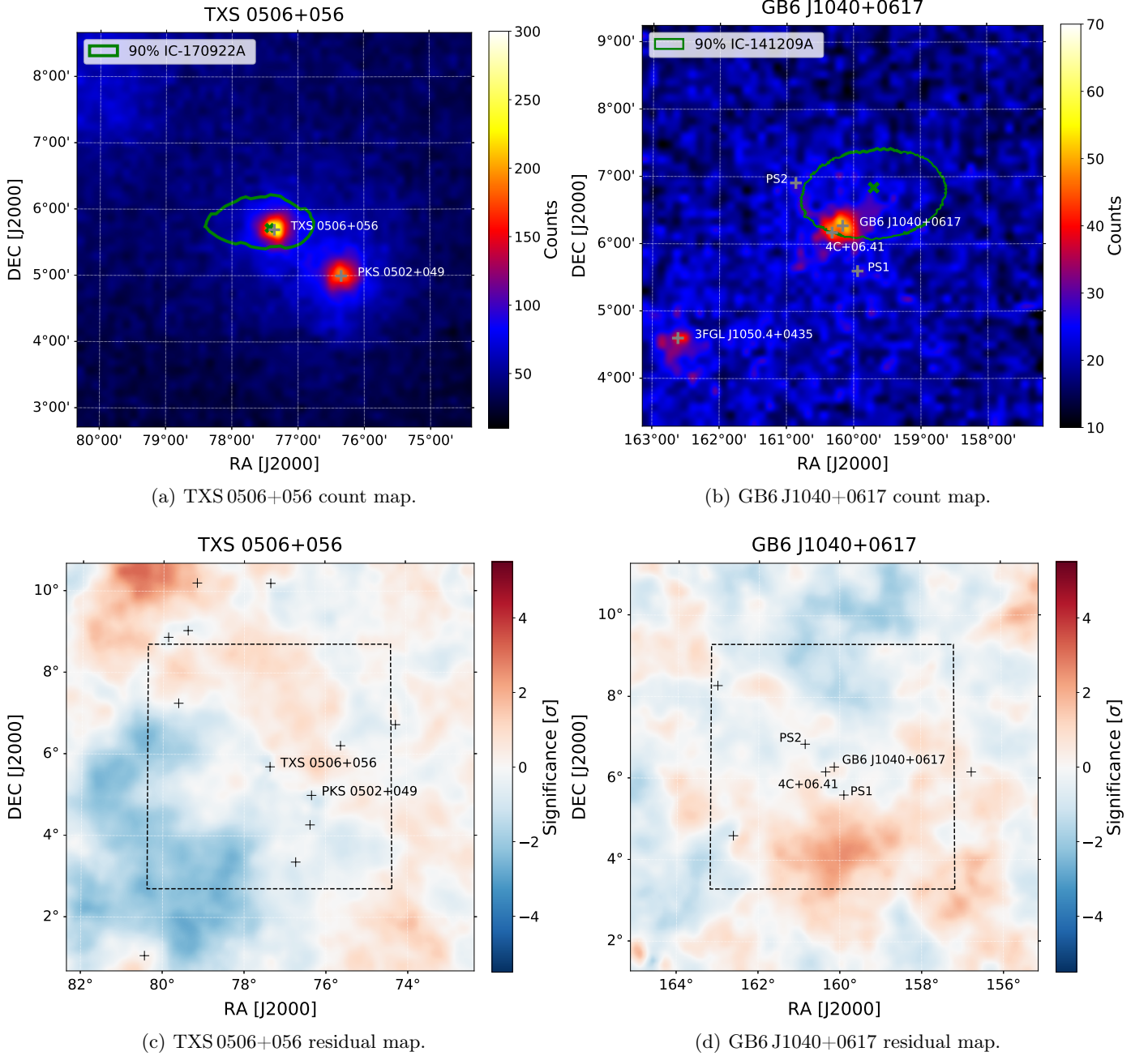


Fig. 1. Top (bottom): count maps (residual maps) >100 MeV of the ROI centered on TXS 0506+056 (left) and GB6 J1040+0617 (right). The 90% neutrino angular uncertainty is shown as green contour in the count maps, the best fit neutrino position is marked by a green "x". Sources modeled in the ROI are marked as black crosses in the residual maps. The residual maps show the entire ROI, while the count maps show a zoom-in to the central region. The zoomed-in region displayed in the count maps is indicated as a dashed black line in the residual maps. The maps are smoothed using a gaussian with standard deviation of 0.1° .

4. IceCube-170922A

On 2017 September 22 at 20:54:30.43 UTC (MJD 58018.87) IceCube detected an extremely high-energy (EHE) through-going muon track event, i.e. IceCube-170922A, with a reconstructed direction of declination (Dec) $5^\circ 72_{-0.30}^{+0.50}$ and right ascension (RA) $77^\circ 43_{-0.65}^{+0.95}$ (J2000 equinox). The traversing muon deposited an energy of (23.7 ± 2.8) TeV in the detector. The primary neutrino energy was estimated to be ~ 290 TeV and the fraction of neutrino events with this energy and arrival direction in

the EHE alert stream that have an astrophysical origin is 56.5% (see Aartsen et al. 2018a, for details).

The gamma-ray blazar TXS 0506+056 is positionally consistent with IceCube-170922A, and it was undergoing a prolonged enhanced emission state at the time of the neutrino detection. This motivated a further search for neutrino emission from the direction of IceCube-170922A, in the whole IceCube archival dataset. A time-dependent analysis of 9.5 years of archival IceCube data (Aartsen et al. 2018b) revealed an excess of detected neutrinos from the direction of TXS 0506+056 between 2014 September and 2015

March, with a post-trials significance of 3.5σ . This excess was found using time-windows of variable width, with both a box-shaped and a Gaussian kernel finding the same excess with comparable significance. The best-fit Gaussian is centered at MJD 57004 with a width corresponding to two times the standard deviation of 110 days and the box function covers the 158-day time range between MJD 56928 and 57086. The fit based on the box function provides a straightforward definition of the start and end times of the fitted neutrino emission. We note that, assuming that the signal is Gaussian, one can show analytically that the optimal box-shaped time window in terms of signal/sqrt(background) is 1.5 times the width of the Gaussian, which matches well with the length of the box time window that was found. In the following, we refer to this excess as the *neutrino flare* and adopt the parameters of the box kernel.

The gamma-ray source TXS 0506+056 at Dec= +5°69, RA= 77°36 lies well within the 50% neutrino error circle at a distance of 0°1 from the best fit neutrino position (see the gamma-ray count map in Fig. 1). The source is listed in the 3FGL as well as 3FHL as 3FGL J0509.4+0541 and 3FHL J0509.4+0541, respectively (Acero et al. 2015; Ajello et al. 2017). The 3FGL catalog is based on gamma-ray data in the energy range of 100 MeV to 300 GeV, whereas the 3FHL catalog is focused on energies above 10 GeV. We note that TXS 0506+056 is also in the 2FHL (Ackermann et al. 2016) catalog based on gamma-ray data above 50 GeV identifying it already as a potential target for very-high-energy gamma-ray emission. TXS 0506+056 is among the brightest 4.4% (5.9%) sources in 3FGL (3FHL) in terms of gamma-ray energy flux within the energy bounds of the corresponding catalog (see also Padovani et al. 2018). We consider the gamma-ray energy flux more likely to be correlated with the neutrino flux than the gamma-ray number flux. Gamma rays accompanying the neutrino production are likely to cascade down to lower energies, not conserving the number flux, but the energy flux. The redshift of TXS 0506+056 was measured to be $z = 0.336$ by Ajello et al. 2014 (later confirmed by Paiano et al. 2018, $z = 0.3365 \pm 0.0010$).

4.1. Spectral Analysis

We analyse 9.6 years of *Fermi*-LAT data in the TXS 0506+056 region starting from 100 MeV. The source-finding algorithm finds one additional source with $TS_{det}^7 > 25$ at a distance of 2°37 from TXS 0506+056. This source is also included in the preliminary 8-year source list, FL8Y, provided by the *Fermi*-LAT collaboration⁸ as FL8Y J0518.4+0715.

In the 3FGL catalog (based on 4 years of data) the SED of the source is modeled with a power-law function. We find that for the almost ten-year data set a log-parabola model is preferred with a test statistic (TS) testing the different spectral shape models of $TS_{SS} = -2(\log \mathcal{L}_{PL} - \log \mathcal{L}_{LP}) = 374.3$ (i.e. the log-parabola model describes the data better with a significance of 19σ). Here \mathcal{L}_{PL} and \mathcal{L}_{LP} are the maximum likelihoods evaluated for the power-law and log-parabola spectral model respectively.

⁷ TS_{det} describes the difference in the maximum $\log \mathcal{L}$ of an ROI model with and without the source.

⁸ FL8Y preliminary source list <https://fermi.gsfc.nasa.gov/ssc/data/access/lat/fl8y/>

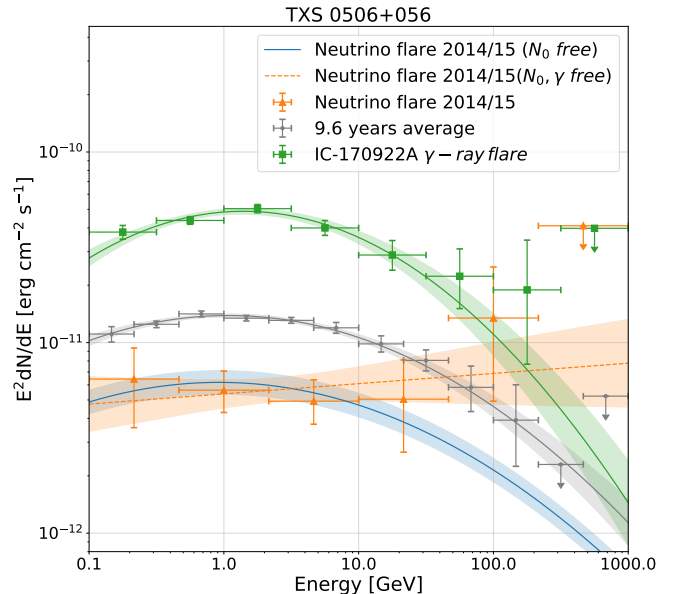


Fig. 2. Spectral energy distribution of TXS 0506+056. *Fermi*-LAT data of the whole 9.6-years range are shown as gray crosses and the best-fit spectral model including statistical uncertainties is overlaid as gray band. Arrows indicate 95% upper limits. The SED of the 2017/18 gamma-ray flare is shown in green. The orange contour shows the SED during the 2014/15 neutrino flare modeled with a power-law function where both normalization and photon index are free to vary. The blue contour shows the log-parabola fit to the 2014/15 dataset, where only the normalization is left free to vary and the spectral parameters α and β are fixed to the 9.6-year average values.

We obtain a best-fit model of $\alpha = 2.03 \pm 0.02$, $\beta = 0.05 \pm 0.01$ and $N_0 = (4.16 \pm 0.08) \times 10^{-12} \text{ cm}^{-2} \text{ s}^{-1} \text{ MeV}^{-1}$ (Fig. 2, gray SED). The scale parameter E_b is fixed to 1.44 GeV.

We follow the standard parameter definitions:

$$\frac{dN}{dE} = N_0 \left(\frac{E}{E_b} \right)^{-(\alpha + \beta \log(E/E_b))} \quad (1)$$

The SED of the neighboring source PKS 0502+049 (Dec=+4°99, RA=76°35, J2000), located 1°23 from TXS 0506+056, is well-modeled by a log-parabola function with best fit values of $\alpha = 2.34 \pm 0.02$, $\beta = 0.10 \pm 0.01$ and $N_0 = (1.08 \pm 0.02) \times 10^{-11} \text{ cm}^{-2} \text{ s}^{-1} \text{ MeV}^{-1}$. Although TXS 0506+056 is less bright than PKS 0502+049 for energies below 1 GeV, its energy flux integrated over the whole analysis energy range results in $(5.10 \pm 0.18) \times 10^{-5} \text{ MeV cm}^{-2} \text{ s}^{-1}$ compared to $(4.18 \pm 0.08) \times 10^{-5} \text{ MeV cm}^{-2} \text{ s}^{-1}$ of the nearby source.

The gamma-ray sky region is well described by the best-fit model, as can be seen in the residual map shown in Fig. 1 (bottom left), which does not show any significant structure.

4.2. Light Curve Analysis

We produce an adaptively-binned (AB) light curve for TXS 0506+056, following the procedure in Lott et al.

(2012). We choose a time binning which yields 15% flux errors in an energy range from 300 MeV⁹ to 1 TeV, and perform a likelihood fit in each bin using a power-law model¹⁰ for TXS 0506+056 while allowing the spectral parameters of the closest neighboring sources to vary. The flux and spectral index variation are shown in Fig. 3.

To identify and characterize statistically-significant variations in the light curve, we apply the Bayesian Block algorithm outlined in Scargle et al. (2013), using the corresponding Astropy implementation¹¹. To determine the optimal value of the prior for the number of blocks, we use the empirical relation evaluated in Scargle et al. (2013) for the probability to falsely report a detection of a change point. This probability, which represents the relative frequency with which the algorithm reports the presence of a change point in data with no signal present, was set to 0.05.

While the largest historical gamma-ray outburst for TXS 0506+056 occurred in 2017 in coincidence with IceCube-170922A (see Fig. 3), the source does not display any remarkable activity during the neutrino flare in 2014/15. Also the gamma-ray spectral shape is compatible with the average over the whole mission. The spectral index shows small variations with respect to the average index of 2.11, and the source shows no obvious extended time periods of hardening or softening, over the full 9.6-year time range.

To further investigate the object's behavior during the neutrino flare, we derive the best-fit model for the region using a time window coincident with the 158-day neutrino excess. We then use the likelihood technique to robustly quantify any potential spectral change of the TXS 0506+056 gamma-ray spectrum with respect to the average one. The likelihood ratio tests the hypothesis H_0 , i.e. the gamma-ray spectral shape is identical to the average one, against the hypothesis H_1 , i.e. an alternative spectral shape. The H_0 model allows only the normalization of TXS 0506+056 to vary in the fit, while the spectral index is fixed to the average values obtained from the 9.6-years analysis. The H_1 has the spectral index of the power-law model for TXS 0506+056 as an additional free parameter. All the other sources in the ROI, along with the Galactic and isotropic diffuse models, have the spectral parameters (including the normalisation) fixed to the 9.6-years fit results for both hypotheses. We define the test statistic to describe spectral change as $TS_{SC} = -2(\log \mathcal{L}_0 - \log \mathcal{L}_1)$, where \mathcal{L}_0 is the likelihood of the whole ROI for the null hypothesis, and \mathcal{L}_1 is the one corresponding to the alternative hypothesis H_1 .

We repeat the analysis for various lower energy thresholds, E_{\min} , of 0.1, 0.5, 1, 2 and 10 GeV and modeling TXS 0506+056 with two different spectral shapes, i.e. power-law and log-parabola. The results are summarized in Table 1. Note that in the case of the log-parabola spectral shape two additional parameters (α and β) are left free in the H_1 model with respect to H_0 ¹². According to

Wilks' theorem the TS distribution can be assumed to follow a χ^2 distribution with one or two degrees of freedom for the power-law or log-parabola spectral model, respectively. The p-value obtained from the χ^2 distribution is converted to a Gaussian equivalent two-sided significance in units of sigma. For all tested cases, the p-value of the spectral change is 4% or greater, providing no significant evidence in favor of a hardening or softening.

Padovani et al. (2018) found a spectral hardening during the neutrino flare in the energy range > 2 GeV with a 2% p-value. In their analysis the lower threshold of > 2 GeV was chosen to avoid source confusion at lower energies with the neighboring source PKS 0502+049. By including the PKS 0502+049 parameters as additional free parameters in our ROI model, we overcome the problem of source confusion, resulting in no significant residuals in the region of the two sources (see Fig. 1). For the specific choice of $E_{\min} = 2$ GeV, we confirm the p-value of 2% found by Padovani et al. (2018) using a power-law model during the 110 days time window given by the width of the Gaussian kernel in the neutrino flare search. In the box window width of 158 days we obtain a slightly lower significance of 2.1σ (p-value of 3.9%) for the same spectral model. For other choices of E_{\min} we find lower significances (see Table 1).

In addition, we investigate possible patterns in the high-energy photons (> 10 GeV) which have a probability of association with TXS 0506+056 of $> 80\%$ ¹³ (see Table 2). Under the hypothesis of a simple correlation between the gamma-ray and neutrino emission in blazars, the highest gamma-ray energies accessible by the LAT may be the best available tracer for high-energy neutrino emission in the absence of TeV gamma-ray observations. During the neutrino flare, we find six photons above 10 GeV, among which two are with energies above 50 GeV. For comparison, we look at the number of expected photons assuming the spectral shape during the non-flaring period of MJD 55800-56500¹⁴ and fitting the normalization in the 158-day time window, obtaining 4.44 (0.69) photons above 10 (50) GeV. We find that the number of high-energy events observed during the neutrino flare is compatible with the typical gamma-ray behavior of TXS 0506+056 during the 9.6 years of LAT monitoring. The small excess of high-energy photons at face value has a p-value of 15% corresponding to a one-sided Gaussian equivalent significance of 1σ . The highest-energy photon associated with TXS 0506+056 over the 9.6-year period was detected on MJD 56819 and has an energy of 159.3 GeV.

A closer investigation of the bright gamma-ray flare in 2017 shows significant structure, which is highlighted by the Bayesian Block algorithm (see Fig. 4). We obtain SEDs for the three brightest sub-flares ranging from MJD 57881-57963, 57983-58062 and 58088-58130 and repeat the search for spectral change applied during the neutrino flare period. We find TS_{SC} values (starting from 100 MeV) of 3.5, 3.4 and 1.77 using a log-parabola function with two extra degrees of freedom pointing to similar spectral shapes

⁹ The lower energy bound corresponds to the decorrelation energy, also referred to as optimum energy, defined in Lott et al. (2012).

¹⁰ On the short time scales considered here, the photon statistics are low and the source is well described by a power-law model.

¹¹ http://docs.astropy.org/en/stable/api/astropy.stats.bayesian_blocks.html

¹² The value of E_b is always fixed, see Massaro et al. (2004)

¹³ This probability is obtained using the method `gtsrcprob` from the Fermi ScienceTools.

¹⁴ The non-flaring period is selected to start after the mild flaring period centered around 55500 and stops before a period of a moderate high-energy flaring activity seen in the lower panel of Fig. 3.

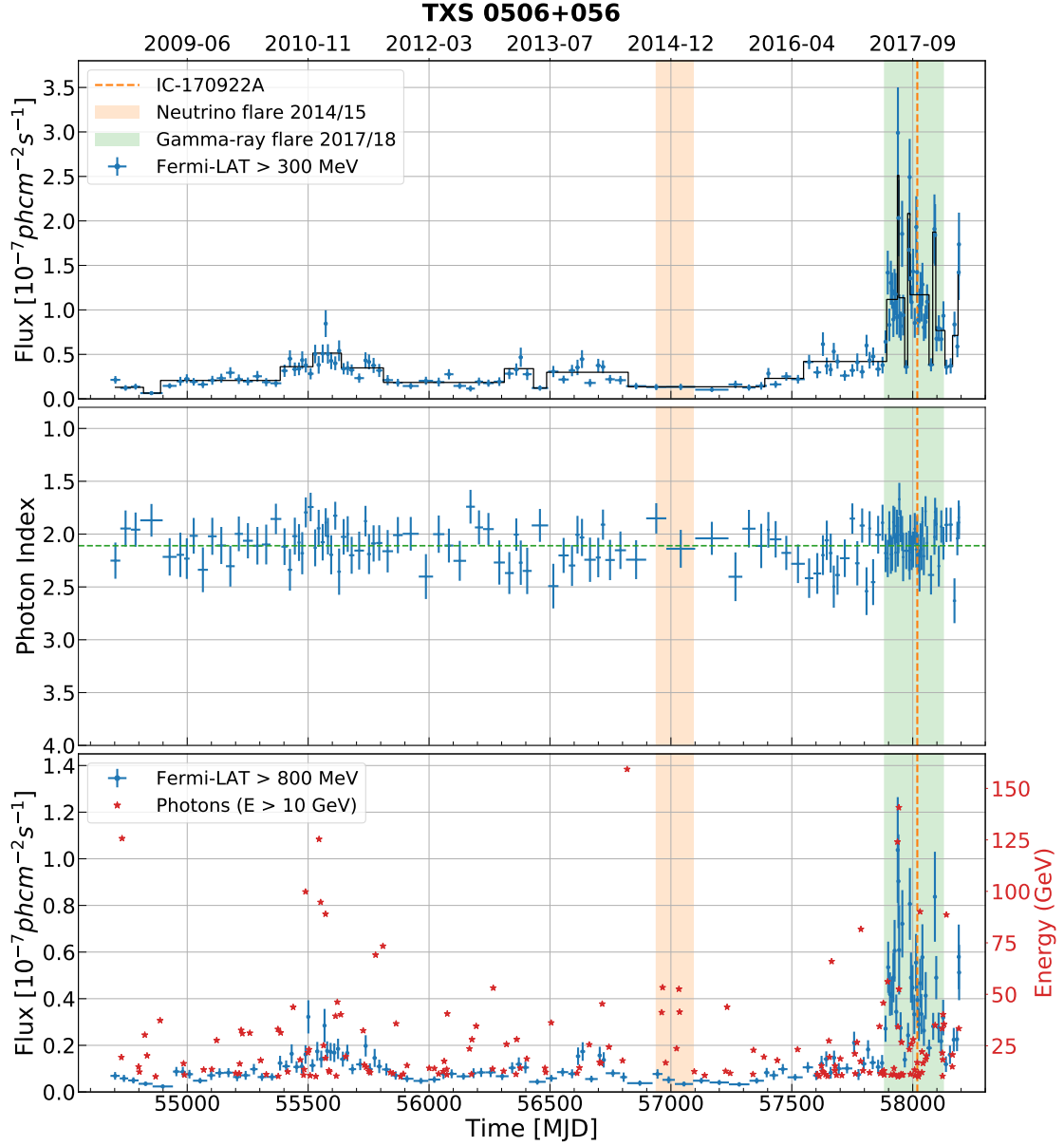


Fig. 3. Adaptive binned light curve for TXS0506+056. The three panels show gamma-ray flux above 300 MeV including the Bayesian Block representation shown in black (panel 1), power-law spectral index (panel 2) and gamma-ray flux above 800 MeV (panel 3). The average spectral index is shown as horizontal dashed green line in panel 2. The third panel additionally includes photons above 10 GeV shown with red stars.

compared to the average 9.6-years SED. The normalization during the sub-flares is 6.09, 6.37 and 5.1 times larger compared to the low-state defined over 700 days. Integrating over the whole flare duration we find 39 (5) photons above 10 GeV (50 GeV), which is compatible with the expected number of photons assuming the average spectral shape and a normalization fitted in the flare time window of 44.37 (4.16).

5. IceCube-141209A

The High-Energy Starting (HESE) muon-track Event IceCube-141209A (event 63 in IceCube Collaboration et al. 2017) was detected on 2014 December 9 at 03:26:04.704 UTC (MJD 57000.14311). To obtain the reconstructed neutrino direction a full likelihood scan is applied on a nar-

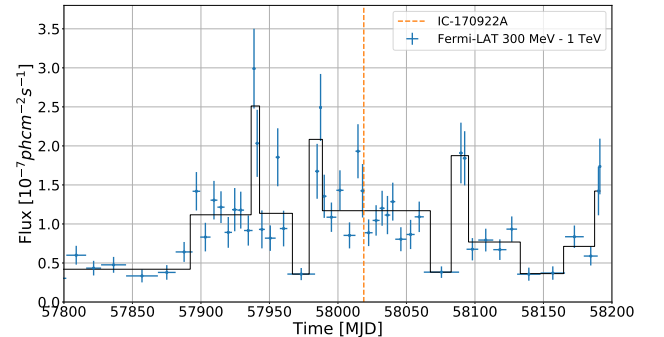


Fig. 4. Zoomed-in gamma-ray light curve of TXS0506+056 around the arrival time of IceCube-170922A (shown in orange) and the bright gamma-ray flare. The black curve shows the result of the Bayesian Block algorithm.

Table 1. Significance of spectral variations during the box time window of the neutrino flare

E_{\min} [GeV]	log parabola			power law			power law index
	TS_{SC}	σ^a	p-value	TS_{SC}	σ^a	p-value	
0.1	2.49	1.06	0.29	1.28	1.13	0.26	1.95 ± 0.12
0.5	4.13	1.53	0.13	3.87	1.97	0.05	1.88 ± 0.13
1.0	2.33	1.01	0.31	1.20	1.09	0.27	1.98 ± 0.17
2.0	5.12	1.77	0.08	4.25	2.06	0.04	1.76 ± 0.20
10.0	3.64	1.40	0.16	2.19	1.48	0.14	1.77 ± 0.40

Notes.^(a) Significance in σ assuming a Gaussian equivalent two-sided probability.**Table 2.** High-energy photons associated with TXS 0506+056 with a probability of $> 80\%$ detected during the neutrino flare time interval

arrival time [MJD]	dist. ^a [°]	energy [GeV]	prob. ^b [%]
56961.908	0.18	41.19	97.18
56965.688	0.02	53.31	99.97
56978.261	0.20	16.77	95.12
57023.479	0.05	23.67	99.90
57033.211	0.09	52.56	99.57
57035.923	0.26	41.40	94.16

Notes.^(a) Angular distance to TXS 0506+056.^(b) Probability to be associated with TXS 0506+056 obtained with `gtsrcprob`.

row grid with about $0^{\circ}06$ distance between the grid points. The resulting map of the likelihood landscape allows us to find the global minimum and the error contours at a given confidence level. The final best fit position and the 90% confidence regions are shown in Fig. 1. The position of the contour line is determined using a simulation of events with similar energy and trajectory through the detector as the event observed, while also varying the modeling of the optical properties of the deep glacial ice within the range allowed by systematic uncertainties, in order to obtain a conservative range. The minimum yields our best estimate of the event direction: Dec= $6^{\circ}84$ and RA= $159^{\circ}70$ (J2000 equinox) and a 90% containment angular uncertainty region of 2.24sqdeg . We note that the best fit location moved and the 90% error region increased with respect to the values published in Aartsen et al. (2018a) and the published event list¹⁵. This is due to updated low-level re-calibrations and an event-by-event treatment of the systematic uncertainties, which are applied to events of special interest such as IceCube-170922A. The updated best-fit location remains within the original 50% localization contour, and does not affect the conclusions in Aartsen et al. (2018a).

The event deposited an energy of $97.4^{+9.6}_{-9.6}$ TeV in the detector. Following the procedure in Aartsen et al. (2017b) we obtain a fraction of neutrinos with this energy and arrival direction in the HESE alert stream of 29%.

Within the 90% error region of IceCube-141209A, we identify only one cataloged gamma-ray source (among all 3FGL and 3FHL sources), 3FGL J1040.4+0615. This is located at a distance of $0^{\circ}70$ from the best-fit neutrino position.

Following the approach presented in Aartsen et al. (2018a)¹⁶, we estimate the p-value of the coincidence with GB6 J1040+0617 by considering the $N_s = 2257$ extragalactic *Fermi*-LAT sources and their monthly light curves. Among all 30-day light curve bins of all sources, 9.5% show a brighter gamma-ray energy flux in the energy range from 1–100 GeV. The area of the 90% neutrino error circle corresponds to $A_\nu = 2.24\text{sqdeg}$. The probability of finding an unassociated brighter source within the error circle is hence $p = N_s A_\nu / (4\pi) \times 0.095 = 1\%$, which corresponds to a Gaussian equivalent one-sided probability of 2.3σ ¹⁷. After correcting for trials introduced by having searched for associations with each of the 37 well-reconstructed high-energy neutrino events in the sample, the final p-value is 30%. In the following we study if the multi-wavelength features of this source indicate a connection to the high-energy neutrino.

The source is included in 3FGL as well as 3FHL as 3FHL J1040.5+0618. We note that it is not included in 2FHL, i.e. it is not a $> 50\text{GeV}$ emitter. It is among the brightest 26.1% (47.0%) 3FGL (3FHL) sources in terms of gamma-ray energy flux, for the 4-year (8-year) integration time. The most likely optical counterpart of this object is SDSS J104031.62+061721.7, located 1 arcmin from the 3FHL position, and associated with the low-synchrotron-peaked (LSP) BL Lac object GB6 J1040+0617. Further analysis of the IceCube-141209A region points out additional significant gamma-ray emission off-set from the direction of GB6 J1040+0617, and consistent with the blazar 4C+06.41. As discussed in the next sections, our detailed investigation indicates that this source awakened in gamma-rays in \sim mid-2015. We find no significant emission observed during the first 7 years of LAT monitoring, including the specific times around the IceCube-141209A detection. During the 9.6 years considered in this work, the brightest persistent gamma-ray emission observed is consistent with the blazar GB6 J1040+0617.

5.1. Gamma-ray region of IceCube-141209A

We perform the same likelihood analysis of the ROI as described in Sec 4. Investigating the 9.6-years gamma-ray events in the vicinity of 3FGL J1040.4+0615, we note signif-

¹⁶ Note that a simplified flat spatial probability density function is applied here in place of a Gaussian representation to accommodate computational constraints associated with the analysis of a large event sample.

¹⁷ Here we assume a uniform distribution of gamma-ray sources neglecting a reduced sensitivity for point source detection along the Galactic plane.

¹⁵ https://icecube.wisc.edu/science/data/TXS0506_alerts

inant gamma-ray emission off-set from the sky direction of GB6 J1040+0617, and positionally consistent with the radio position of the bright flat-spectrum radio quasar 4C+06.41, at redshift 1.27 (Snellen et al. 2002). This object is located at a distance of 0°22 from GB6 J1040+0617 and is neither in the 3FGL catalog nor the FL8Y list. In the second *Fermi*-LAT source catalog of AGN (Acero et al. 2015), 4C+06.41 was tentatively associated with the gamma-ray object 2FGL J1040.7+0614.

In our ROI model, we therefore replace the single source 3FGL J1040.4+0615 with two point-like sources located at the radio positions of GB6 J1040+0617 and 4C+06.41 (Gregory et al. 1996; Lambert & Gontier 2009). Integrating over the whole 9.6-year LAT dataset, 4C+06.41 is detected with a TS_{det} of 36, while GB6 J1040+0617 dominates the bulk of the observed gamma-ray emission with a TS_{det} of 277. An examination of the temporal behavior of these objects in gamma rays is presented in section 5.2 and helps disentangling the gamma-ray emission observed from this region of the sky.

Furthermore, two additional new sources are found in the gamma-ray ROI, Fermi J1039.7+0535 and Fermi J1043.4+0654. This is not surprising given the longer integration time of our study with respect to the *Fermi*-LAT catalog (more than double the 3FGL one). In the counts map in Fig. 1 we refer to those sources as PS1 and PS2, respectively. PS2 is also included in FL8Y as FL8Y J1043.4+0651 and associated with the BL Lac object 5BZB J1043+0653. PS1 and PS2 are dim sources with TS_{det} values of 36.85 and 26.27 in the 9.6-year data set. They are adequately modeled by power-law spectra with best-fit spectral indices of 2.11 ± 0.17 and 1.80 ± 0.21 , respectively. Both gamma-ray sources lie outside of the IceCube 90% error contour. Based on the faintness of these sources and distance from the IceCube event, we do not investigate them further here.

Investigating the gamma-ray region of IceCube-141209A, we note two bright sources: 3FGL J1050.4+0435 detected with a TS_{det} of 463, located 3°0 away from GB6 J1040+0617; and 3FGL J1058.5+0133, detected with a TS_{det} of 8619, located 6°5 from GB6 J1040+0617. Since their gamma-ray flux is comparable to GB6 J1040+0617, we let their spectral parameters free to vary in the likelihood fit.

5.2. Gamma-ray light curve of GB6 J1040+0617

The adaptively-binned light curve starting at the optimal energy of 300 MeV of GB6 J1040+0617 highlights several gamma-ray flux variations, observed throughout the 9.6 years (see Fig. 5). The most clearly identified feature is a bright hard-spectrum state that lasts 721 days, from MJD 55753 to MJD 56474. During that state the source has a peak flux value of $2.8 \pm 0.6 \times 10^{-8} \text{ ph cm}^{-2} \text{ s}^{-1}$ integrated in the energy range from 300 MeV to 1 TeV (a factor of 2.5 increase compared to the average flux) and an average power-law index of 2.08 ± 0.04 . The source shows an increased activity that starts a few days before the IceCube-141209A detection and lasts 93 days, from MJD 56997 to 57090. The duration of this flare is defined by the bin edges of the two high-flux adaptively-binned time bins.

Fig. 6 (left) shows the SED averaged over the time window from MJD 54633 to 57227 (where we have a significant detection of GB6 J1040+0617 with TS_{det} of 451) compared

to the hard bright state and to the SED during the 93 days around the neutrino arrival time. The average gamma-ray emission is well modeled by a power law with $\gamma = 2.26 \pm 0.04$ and $N_0 = 1.77 \pm 0.08 \times 10^{-12} \text{ cm}^{-2} \text{ s}^{-1} \text{ MeV}^{-1}$. A likelihood ratio test similar to the one performed in Sec. 4.2 shows a hardening of the spectrum during the hard bright state at the 4.1σ level. Furthermore we find that the spectral shape during the hard state favors a log-parabola instead of a power-law model, with best-fit spectral parameters $\alpha = 2.03 \pm 0.06$ and $\beta = 0.10 \pm 0.03$ (E_b is fixed to 1 GeV) with a 19σ significance. We note that, during the bright hard state, there is an increase of at least a factor of 10 in the energy at which the high-energy component of the SED peaks.

During the 93-day window around the neutrino arrival time the source is brighter by a factor of 2.4 compared to the average integrated energy flux with a spectral shape compatible to the average one at one-sigma level. The best fit spectral parameters during this time are $\gamma = 2.43 \pm 0.11$ and $N_0 = 3.76 \pm 0.55 \times 10^{-12} \text{ cm}^{-2} \text{ s}^{-1} \text{ MeV}^{-1}$.

We do not find photons above 50 GeV during the 9.6 years of *Fermi*-LAT observations, consistent with the source not being included in the 2FHL catalog. During the bright hard state we find 10 photons above 10 GeV, which is compatible with 9.56 expected photons from the average spectral shape with fitted normalization during the flare time. We do not find an excess in high-energy photons because the spectral change is mainly due to a lack in low-energy photons caused by a shift in the high-energy SED peak to higher energies. We find one photon with energy larger than 10 GeV during the flare at the neutrino arrival time, which is consistent with the expectation of 1.54 photons obtained assuming the average spectral shape with fitted normalization during the flare time.

5.3. Gamma-ray light curve of 4C+06.41

Fig. 7 shows the adaptive binned light curve for 4C+06.41 starting at the optimal energy of 170 MeV beginning at MJD 57228. At earlier times no significant emission of the source is detected. The emission in the time window from MJD 57228-58193 is well modeled by a power law with best-fit parameters $\gamma = 2.73 \pm 0.05$, $N_0 = (2.05 \pm 0.16) \times 10^{-13} \text{ cm}^{-2} \text{ s}^{-1} \text{ MeV}^{-1}$ and reaches a TS_{det} of 322.

At the arrival time of IceCube-141209A the gamma-ray flux is below $1.44 \times 10^{-9} \text{ ph cm}^{-2} \text{ s}^{-1}$ at 95% confidence level, integrated in the energy range from 300 MeV to 1 TeV. The source is in flaring state during a 95-day period between MJD 57729 to 57824 where it outshines GB6 J1040+0617 which is not significantly detected. During the flare the source follows a power-law spectrum with best-fit parameters $\gamma = 2.61 \pm 0.07$ and $N_0 = (7.01 \pm 0.75) \times 10^{-12} \text{ cm}^{-2} \text{ s}^{-1} \text{ MeV}^{-1}$.

5.4. Disentangling the Gamma-ray Emission

The light curves presented in Fig. 5 and Fig. 7 indicate that the gamma-ray emission from GB6 J1040+0617 dominates at earlier times, up to ~mid-2015 when the object turned into a quiescent gamma-ray state, mostly below the detection sensitivity for the LAT. Mid-2015 is also the time around which 4C+06.41 starts to emit a detectable gamma-ray flux. To prove that the temporal coincidence of the on-

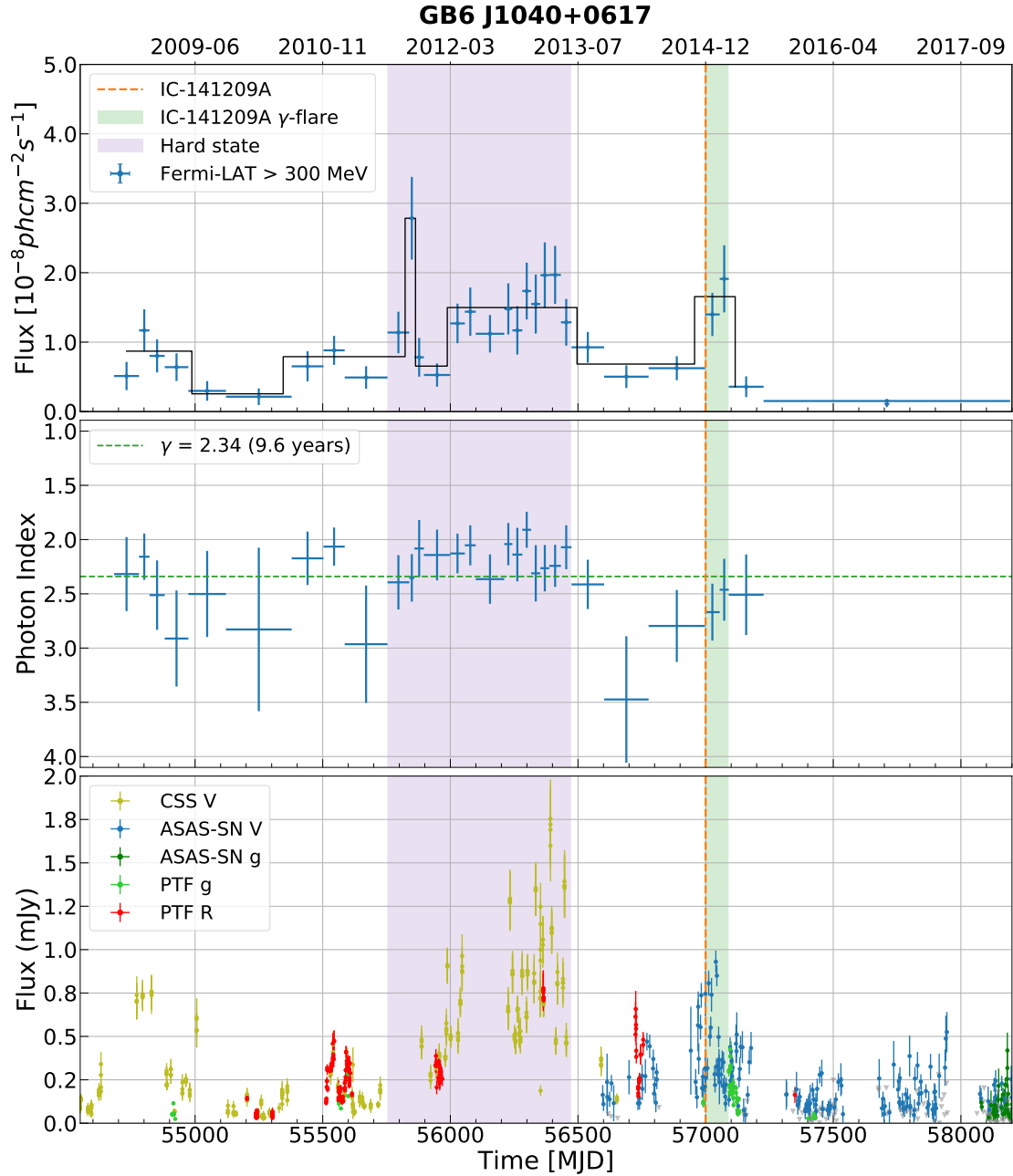


Fig. 5. Adaptively-binned light curve for GB6 J1040+0617. The first two panels show gamma-ray flux above 300 MeV including the Bayesian Block representation shown in black (panel 1) and power-law spectral index (panel 2). In the last time bin the source is not detected significantly, therefore a 95% flux upper limit is shown in panel 1. In that case the spectral index cannot be fitted. The average spectral index is overlaid as a horizontal green dashed line. The third panel shows optical data obtained from ASAS-SN, PTF and CSS. ASAS-SN upper limits are displayed as gray triangles. The arrival of IceCube-141209A is indicated as an orange dashed line. The purple shaded region marks the bright and hard gamma-ray state, while the green shaded region indicates the gamma-ray flare in coincidence with the neutrino arrival time.

set of the gamma-ray emission of 4C+06.41 and the drop in gamma rays from GB6 J1040+0617 is not due to source confusion at low energies, we repeat the analysis at $>1\text{GeV}$ (not shown). Here the improved LAT PSF minimizes the risk of source confusion. We retrieve similar results at high-energies showing the robustness of our analysis.

The radio-loud object SDSS J104039.54+061521.5 is located at RA, Dec = 160°16475, 6°2558, just 1 arcmin away from the radio position of GB6 J1040+0617. Figure 8 shows the best-fit gamma-ray localization, position and 99% error, for two putative sources called GB6-Fermi and 4C-Fermi,

using the best statistics available (full 9.6-years dataset). We find that the best-fit gamma-ray positions (blue cross for the first and black for the second) coincide well with the radio positions of GB6 J1040+0617 and 4C+06.41 respectively (green and orange cross). SDSS J104039.54+061521.5 is located outside of both the 99% error circles (blue circle) and is thus excluded as responsible for the majority of the prolonged gamma-ray emission observed by the LAT. Adding another putative source at the radio position of SDSS J104039.54+061521.5 in our ROI does not significantly improve our model, yielding a significance of

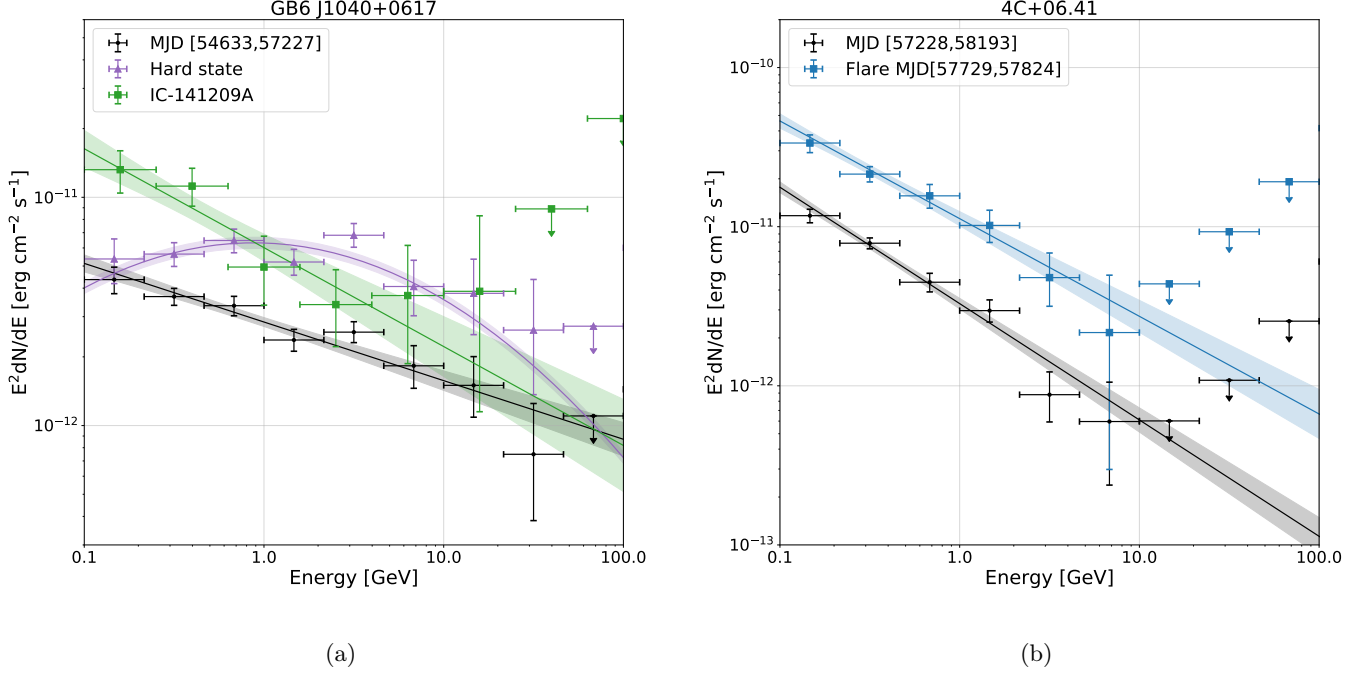


Fig. 6. Spectral energy distributions of GB6 J1040+0617 and 4C+06.41. *Fermi*-LAT data of the respective time ranges when each source is significantly detected are shown as black crosses, arrows indicate 95% upper limits and the best-fit spectral model including statistical uncertainties is overlaid as a black band. Left: average SED of GB6 J1040+0617 compared to the SED during the 93-day gamma-ray excess coincident with the neutrino detection and the bright hard state during MJD 55753-56474. Right: average SED of 4C+06.41 compared with the SED during the bright gamma-ray flare during MJD 57729-57824.

$TS_{det} = 0$ for SDSS J104039.54+061521.5. We calculate a 95% flux upper limit for SDSS J104039.54+061521.5 of $8.8 \times 10^{-10} \text{ ph cm}^{-2} \text{ s}^{-1}$ for a power-law spectral shape with index of 2.0 integrated over the energy range from 100 MeV to 1 TeV.

As a sanity check, we run a dedicated analysis for the flaring time intervals to derive the best-fit localization of the gamma-ray emission. We find that the bright hard state and the modest flare around the neutrino arrival time are consistent with the position of GB6 J1040+0617 while the most recent enhanced gamma-ray emission is positionally consistent with 4C+06.41 (see Fig. 9). This is supported by the softer spectral shape observed during the most recent flare, matching well the one of 4C+06.41 (see Fig. 6). The association of the different flaring states to the two sources is supported by the temporal behavior of the two sources in optical wavelength (see Sec. 5.5). Since 4C+06.41 does not show any significant gamma-ray emission at the arrival time of IceCube-141209A, we focus here on GB6 J1040+0617 for closer multi-wavelength study.

5.5. Multi-wavelength data collection

Archival observations of the gamma-ray sources in the IceCube-141209A region are available for several wavelengths.

Optical data in the V-band and g-band from the All-Sky Automated Survey for Supernovae (ASAS-SN, Shappee et al. 2014; Kochanek et al. 2017) are processed by the fully automatic ASAS-SN pipeline using the ISIS image subtraction package (Alard & Lupton 1998; Alard 2000).

We remove science images by eye that are obviously affected by clouds. We then perform aperture photometry on the subtracted science image using the IRAF *apphot* package, adding back in the flux from the reference image. The photometry is calibrated using the AAVSO Photometric All-Sky Survey (APASS; Henden et al. 2015). Additional V-band data from the Catalina Sky Survey (CSS, Drake et al. 2009) are available from the public database and are based on aperture photometry. R and g band light curves from the Palomar Transient Factory (PTF) are obtained from the IPAC archive (Laher et al. 2014; Masci et al. 2017) and processed using forced PSF-fit photometry (Masci et al. 2017) on the subtracted images adding back the flux from the reference image. The long term optical light curve of GB6 J1040+0617 shown in the lower panel of Fig. 5 shows a similar flux variability pattern when compared to the gamma-ray light curve, including an excess coincident with the arrival of IceCube-141209A.

The optical light curve of 4C+06.41, recorded by ASAS-SN and processed as outlined above, shows a mild excess around MJD 57800 in coincidence with the gamma-ray flare attributed to 4C+06.41 (see Sec. 5.2). The OVRO radio light curve shows a very slow rise starting around MJD 56700 and peaks almost one year before the gamma-ray flare.

Fig. 10 shows an SED of GB6 J1040+0617 compiled from archival data. Note that these data are not contemporaneous. X-ray data are taken from the third XMM-*Newton* serendipitous source catalog (Rosen et al. 2016) and the *Swift* XRT point source catalog (Evans et al. 2014). We observe a flux offset in the *Swift*-XRT and XMM-*Newton*

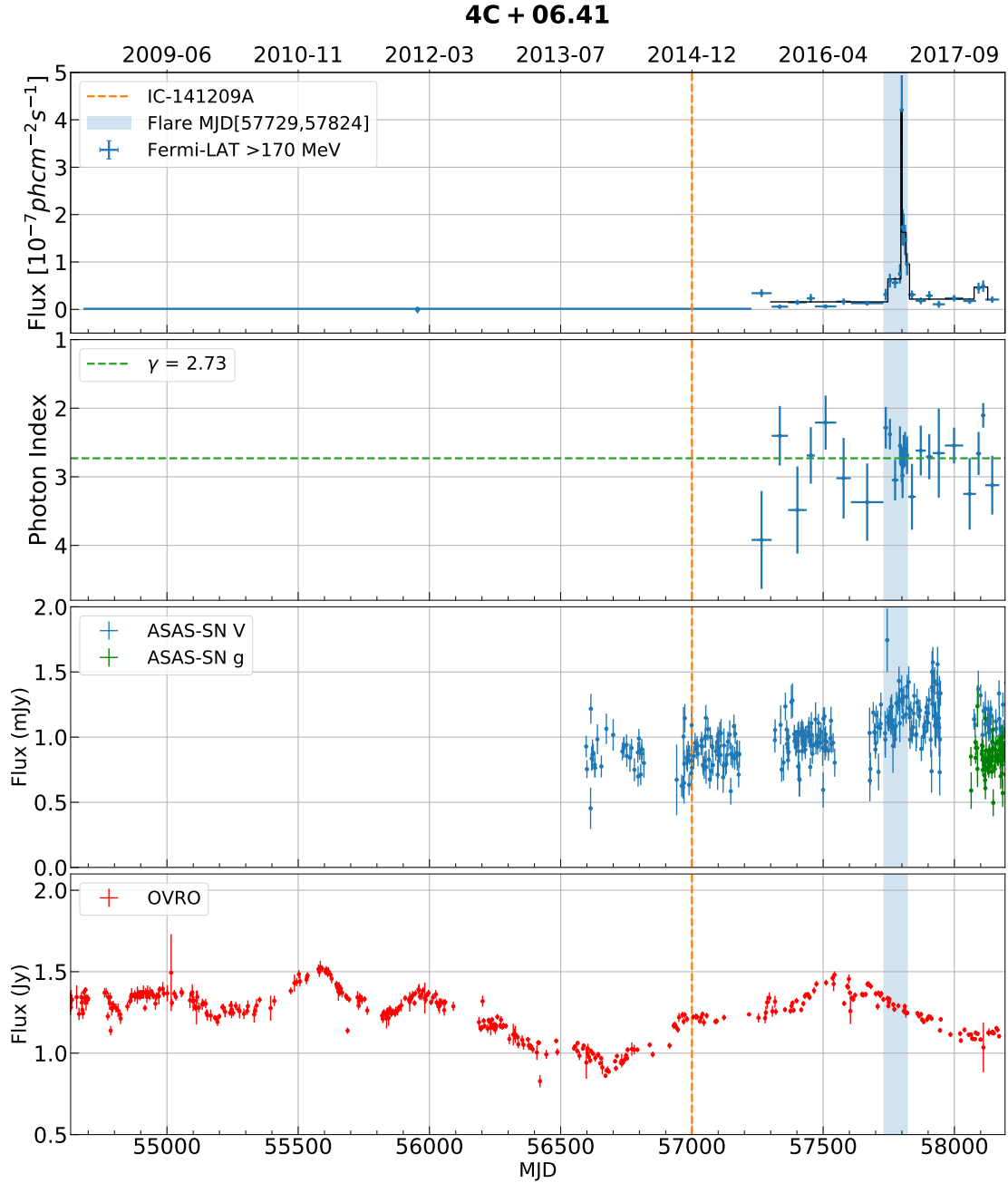


Fig. 7. Adaptively-binned light curve for 4C+06.41. The first two panels show gamma-ray flux above 170 MeV including the Bayesian Block representation shown in black (panel 1) and power-law spectral index (panel 2). In the first time bin the source is not detected significantly, therefore a 95% flux upper limit is shown in panel 1. In that case the spectral index cannot be fitted. The average spectral index is overlaid as a green line. The third panel shows optical data obtained from ASAS-SN, and the fourth panel shows radio data from OVRO. The arrival of IceCube-141209A is indicated as an orange line.

data, which we attribute to different observation periods. *XMM-Newton* data were collected in 2003 May while *Swift*-XRT observed the source between 2007 and 2011. Radio data come from the GB6 catalog of radio sources (Gregory et al. 1996) and the FIRST survey (Helfand et al. 2015). Optical data are obtained from SDSS (Abolfathi et al. 2018) and far and near UV observations from *GALEX* (Bianchi et al. 2017). Infrared data are obtained from *WISE* (Wright et al. 2010). The SED shows the typical two-hump structure with the high-energy peak at ~ 100 MeV and the low-energy peak in the infrared around 0.1 eV, which makes it a low-peaked synchrotron source.

6. Conclusions

High-energy neutrino production in blazars is accompanied by the production of gamma rays at similar energies. While the neutrinos escape from the system, the gamma rays can interact and cascade down to lower energies. Sources bright at GeV gamma rays are capable of accelerating particles to high energies and thus may be good tracers for neutrino emission. This paper presents a detailed characterization of the gamma-ray behavior for the potential electromagnetic counterparts spatially consistent with two well-

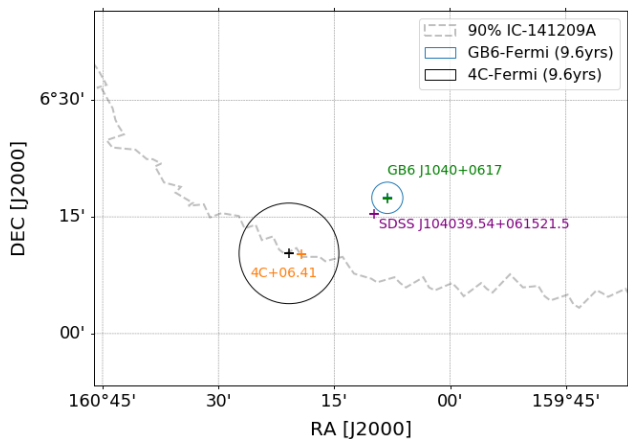


Fig. 8. Gamma-ray best-fit positions: the blue and black circles indicate the 99% containment radius of the gamma-ray positions of the two putative sources GB6-Fermi and 4C-Fermi. The 90% neutrino error circle is shown as dashed gray line for reference. Orange, green and violet crosses indicate the radio positions of the blazars located in the region.

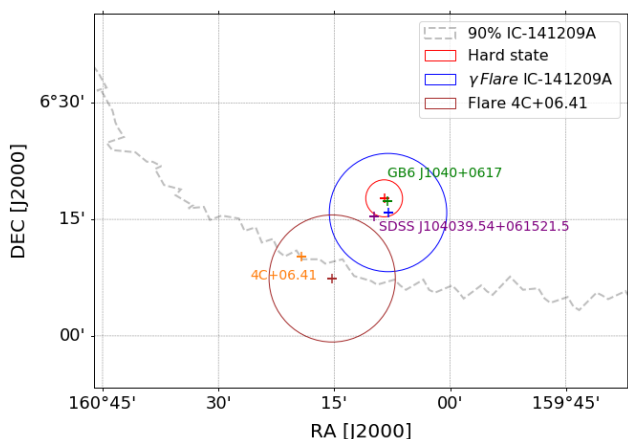


Fig. 9. Gamma-ray flare positions: the bright hard state and modest flare at the arrival of IceCube-141209A are shown in red and blue respectively, while the late flare attributed to 4C+06.41 is shown in brown. The circles indicate the 99% containment radius of the gamma-ray position. The 90% neutrino error circle is shown as dashed gray line.

reconstructed IceCube neutrinos put into a multi-frequency perspective.

6.1. IceCube-170922A gamma-ray counterpart

In Aartsen et al. (2018a) TXS 0506+056 has been suggested as the counterpart of IceCube-170922A. The refined gamma-ray analysis presented here confirms that at the time of the neutrino detection this blazar was undergoing a major, prolonged gamma-ray outburst phase without significant spectral variations. However, during the time of the 2014/15 neutrino flare reported in Aartsen et al. (2018b), we find neither an excess of gamma rays nor a significant gamma-ray spectral change with respect to the average. This could point to absorption of the gamma rays (Liu et al. 2018) or to an increase in the injection of protons, potentially explainable by hybrid models as the one proposed by e.g. Gao et al. 2018; Murase et al. 2018. Reimer et al. (2018) have conducted a detailed investigation of the

electromagnetic signal expected for photo-hadronically produced neutrinos in 2014/15 by TXS 0506+056. Comparing simulations to the observed data, they show that the link between gamma rays and neutrinos in this blazar may not be trivial. They derive the conclusion that in most of the considered scenarios the observed high-energy photons and neutrinos may be not casually connected.

The bright gamma-ray flare in 2017 coincident with IceCube-170922A shows significant variations on short time scale (see Fig. 4). While the source is detected with high confidence on daily time scale, significant variations are only found on a weekly timescale (by the Bayesian Block algorithm). However, fast variability on 1-day time scale was found in > 100 GeV gamma rays by MAGIC (Ansoldi et al. 2018) and points to a compact emission region.

6.2. IceCube-141209A gamma-ray counterpart candidates

If IceCube-141209A is astrophysical in origin, then the low-synchrotron peaked gamma-ray blazar GB6 J1040+0617 appears to be the most likely counterpart, assuming a direct correlation between the gamma-ray and neutrino emission. Under that assumption the neighboring FSRQs 4C+06.41 and SDSS J104039.54+061521.5 are less favored as the likely neutrino counterpart, because no significant high-energy emission was detected at the arrival of IceCube-141209A. However, in models that assume a different scaling of the neutrino flux with the electromagnetic emission, 4C+06.41 and SDSS J104039.54+061521.5 may be considered as potential neutrino counterparts (e.g. Stecker et al. 1991; Murase et al. 2016; Reimer et al. 2018).

The variability pattern of GB6 J1040+0617 displays major and minor flaring episodes in both gamma-ray and optical wavelengths. At the detection time of IceCube-141209A the blazar showed an increase in the gamma-ray flux over 93 days, with respect to the 9.6 years averaged flux (Fig. 5, panel 1). A Bayesian block analysis confirms the flaring activity. However, the bulk of the > 300 MeV gamma-ray energy output is observed during the 721-day long high-flux state before the neutrino detection, as evidenced by the light curve shown in Fig. 5 (panel 1). The source entered a lower active state roughly 100 days after the neutrino arrival.

Enhanced activity contemporaneous to IceCube-141209A is also supported by an overall steady increase in the object's flux in the optical band (Fig. 5, panel 3). Simultaneous ASAS-SN observations confirm that, at the neutrino detection time, the blazar's optical flux was higher than average, and displayed the second brightest historical value (while the record-holder was the optical flare coincident with the bright hard gamma-ray state). A zoom-in of the optical light curve around the neutrino arrival time (Fig. 11) shows an increase compared to the low state by almost a factor of 10. We do not find a hint for fast gamma-ray variability during this period, while short-timescale flux variations were evident in the optical band. This could be compatible with the proton-synchrotron scenario discussed in Zhang et al. (2018). However, low gamma-ray statistics and the lack of polarization information prevents us from probing the model predictions.

Assuming a redshift of 0.73, with the caveats mentioned earlier, the rest-frame energetics of GB6 J1040+0617 are similar to those of TXS 0506+056. The average gamma-ray luminosity between 100 MeV and 100 GeV

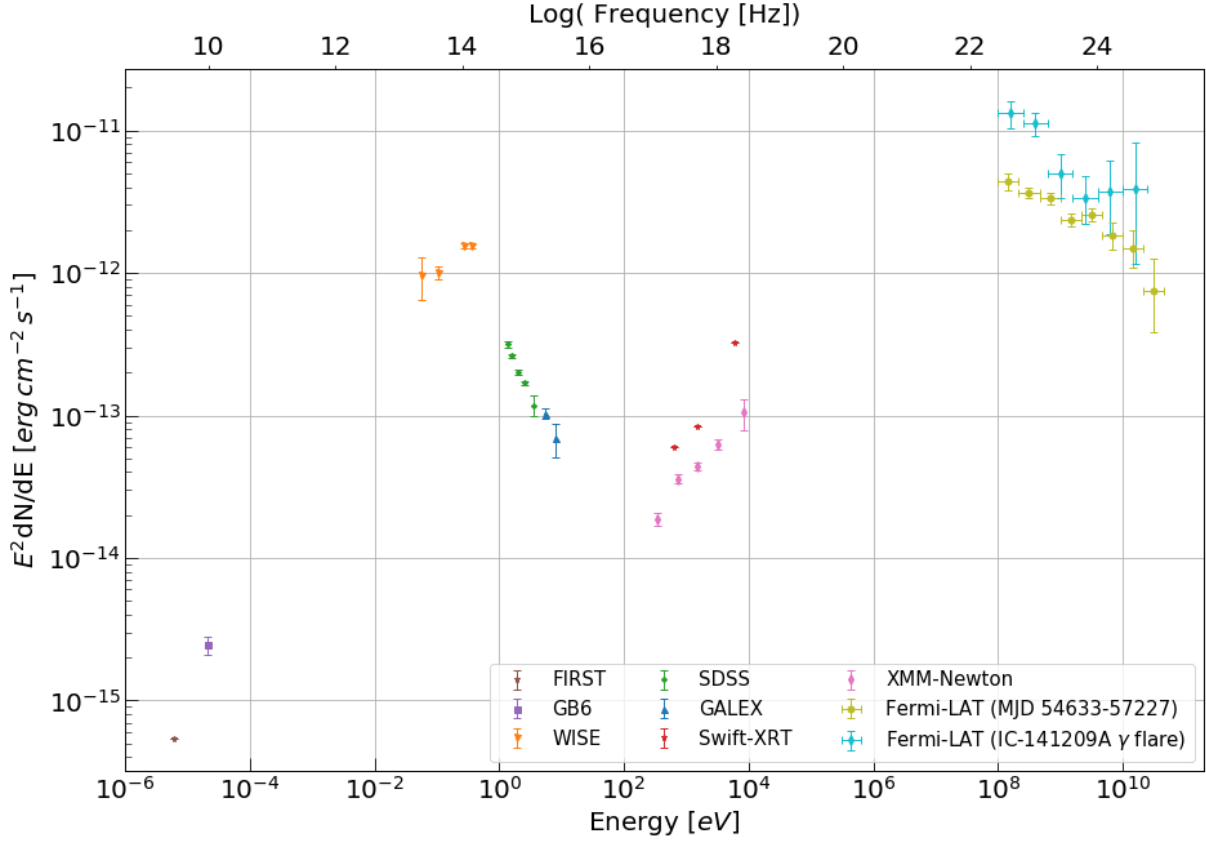


Fig. 10. Multi-wavelength SED in the observer frame for GB6 J1040+0617 using archival data, which are not contemporaneous.

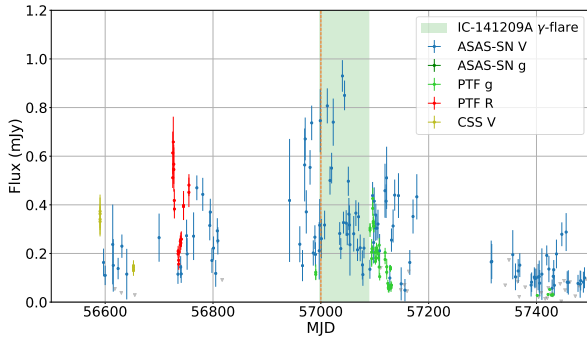


Fig. 11. Zoomed in optical light curve of GB6 J1040+0617 around the arrival time of IceCube-141209A (shown in orange). The green shaded region indicates the gamma-ray flare in coincidence with the neutrino arrival time (see Fig. 5).

was 4.1×10^{46} erg/s, which is 1.5 times larger than TXS 0506+056 (Aartsen et al. 2018a)¹⁸. The modest flare at the arrival of IceCube-141209A had a luminosity of 8.9×10^{46} erg/s.

We perform a rough estimate of the expected neutrino event rate assuming that the average neutrino flux reaches

at most the level of the gamma-ray flux. In hybrid models the X-ray flux should be dominated by the hadronic component (e.g. Gao et al. 2018; Keivani et al. 2018) and therefore for our rough estimate we assume that the neutrino flux has to be higher than the X-ray flux. We assume a peak gamma-ray flux of $E^2 dN/dE \approx 5 \times 10^{-12}$ erg cm⁻² s⁻¹, a minimum X-ray flux of $E^2 dN/dE \approx 2 \times 10^{-14}$ erg cm⁻² s⁻¹ and a neutrino spectral shape of E^{-2} . We use the IceCube effective area at the declination of GB6 J1040+0617 (which is similar to the effective area published in Aartsen et al. (2018b) for TXS 0506+056 using the 86-string configuration of 2015 May 18 to 2017 October 31). We find an optimistic expected number of neutrinos between 100 GeV and 10 PeV of 1.8 events per year and 0.7 events above 100 TeV for a neutrino flux as high as the peak gamma-ray flux and a pessimistic number of 0.01 per year between 100 GeV and 10 PeV and 0.003 per year above 100 TeV. An expectation value much smaller than one is compatible with the detection of a single high-energy event due to the Eddington bias discussed in Strotjohann et al. (2018). This shows that GB6 J1040+0617 is a plausible neutrino-source candidate and motivates the search for TeV neutrinos at this source position similar to the one performed at the position of TXS 0506+056 (Aartsen et al. 2018b), which is in preparation.

¹⁸ Note that with an average redshift of *Fermi*-LAT BL Lacs of $z = 0.3$ the estimated luminosity of GB6 J1040+0617 reduces to 4.9×10^{45} erg/s.

6.3. Gamma-ray blazars as neutrino source population

Only two of the 37 well reconstructed high-energy neutrino events satisfying the realtime trigger criteria are found to be positionally consistent with sources in the *Fermi*-LAT energy range. Finding two out of 18.5 ± 1.8 events¹⁹ originating from *Fermi* blazars is consistent with the blazar stacking limit performed in Aartsen et al. (2017b) constraining the blazar contribution to the measured diffuse neutrino flux to $< 30\%$.

Both TXS 0506+056 and GB6 J1040+0617 share similar properties: they belong to the BL Lac class, the former to the sub-sample of ISP and the latter to the one of LSP sources, and have comparable gamma-ray luminosities. Moreover, they are located at a similar declination, near the equatorial plane, which is viewed along the horizon from the South Pole. This is the sky region for which IceCube is most sensitive to high-energy neutrinos. While we do not have significant evidence that IceCube-141209A is associated with any of the gamma-ray objects identified in its vicinity, our multi-wavelength study suggests that based on its gamma-ray properties, GB6 J1040+0617 remains a plausible candidate for being a gamma-ray counterpart to the neutrino event. However, given the currently limited knowledge of the blazar jet properties and acceleration mechanisms leading to an uncertainty in the scaling of the neutrino flux with the electromagnetic emission and the lack of simultaneous multi-wavelength data, SDSS J104039.54+061521.5 and 4C+06.41 cannot be ruled out as possible counterparts of IceCube-141209A.

This work points to the importance of broad-band multi-wavelength and multi-messenger data to provide us with a more complete understanding of candidate neutrino counterparts. These will be a crucial ingredient in future searches for neutrino emitters, and hence cosmic-ray source populations.

Acknowledgements. **Fermi-LAT:** The *Fermi* LAT Collaboration acknowledges generous ongoing support from a number of agencies and institutes that have supported both the development and the operation of the LAT as well as scientific data analysis. These include the National Aeronautics and Space Administration and the Department of Energy in the United States, the Commissariat à l’Energie Atomique and the Centre National de la Recherche Scientifique / Institut National de Physique Nucléaire et de Physique des Particules in France, the Agenzia Spaziale Italiana and the Istituto Nazionale di Fisica Nucleare in Italy, the Ministry of Education, Culture, Sports, Science and Technology (MEXT), High Energy Accelerator Research Organization (KEK) and Japan Aerospace Exploration Agency (JAXA) in Japan, and the K. A. Wallenberg Foundation, the Swedish Research Council and the Swedish National Space Board in Sweden. Additional support for science analysis during the operations phase is gratefully acknowledged from the Istituto Nazionale di Astrofisica in Italy and the Centre National d’Études Spatiales in France. This work performed in part under DOE Contract DE-AC02-76SF00515. SG and AF are supported by the Initiative and Networking Fund of the Helmholtz Association. SB was supported by the NASA Postdoctoral Program. **ASAS-SN:** The ASAS-SN team thanks the Las Cumbres Observatory and its staff for its continuing support of the ASAS-SN project. ASAS-SN is supported by the Gordon and Betty Moore Foundation through grant GBMF5490 to the Ohio State University and NSF grant AST-1515927. Development of ASAS-SN has been supported by NSF grant AST-0908816, the Mt. Cuba Astronomical Foundation, the Center for Cosmology and AstroParticle Physics at the Ohio State University, the Chinese Academy

of Sciences South America Center for Astronomy (CASSACA), the Villum Foundation, and George Skistos. J.F.B. is supported by NSF Grant No. PHY-1714479. **IceCube:** The IceCube collaboration provided the analysis of IceCube-141209A via significant contributions by Claudio Kopper. The IceCube collaboration gratefully acknowledges the support from the following agencies and institutions: USA – U.S. National Science Foundation-Office of Polar Programs, U.S. National Science Foundation-Physics Division, Wisconsin Alumni Research Foundation, Center for High Throughput Computing (CHTC) at the University of Wisconsin-Madison, Open Science Grid (OSG), Extreme Science and Engineering Discovery Environment (XSEDE), U.S. Department of Energy-National Energy Research Scientific Computing Center, Particle astrophysics research computing center at the University of Maryland, Institute for Cyber-Enabled Research at Michigan State University, and Astroparticle physics computational facility at Marquette University; Belgium – Funds for Scientific Research (FRS-FNRS and FWO), FWO Odysseus and Big Science programmes, and Belgian Federal Science Policy Office (Belspo); Germany – Bundesministerium für Bildung und Forschung (BMBF), Deutsche Forschungsgemeinschaft (DFG), Helmholtz Alliance for Astroparticle Physics (HAP), Initiative and Networking Fund of the Helmholtz Association, Deutsches Elektronen Synchrotron (DESY), and High Performance Computing cluster of the RWTH Aachen; Sweden – Swedish Research Council, Swedish Polar Research Secretariat, Swedish National Infrastructure for Computing (SNIC), and Knut and Alice Wallenberg Foundation; Australia – Australian Research Council; Canada – Natural Sciences and Engineering Research Council of Canada, Calcul Québec, Compute Ontario, Canada Foundation for Innovation, WestGrid, and Compute Canada; Denmark – Villum Fonden, Danish National Research Foundation (DNRF); New Zealand – Marsden Fund; Japan – Japan Society for Promotion of Science (JSPS) and Institute for Global Prominent Research (IGPR) of Chiba University; Korea – National Research Foundation of Korea (NRF); Switzerland – Swiss National Science Foundation (SNSF). **Others:** The authors thank Matthias Kadler, Anatoli Fedynitch and Shan Gao for fruitful discussions. The CSS survey is funded by the National Aeronautics and Space Administration under Grant No. NNG05GF22G issued through the Science Mission Directorate Near-Earth Objects Observations Program. The CRTS survey is supported by the U.S. National Science Foundation under grants AST-0909182. This research has made use of data from the OVRO 40-m monitoring program (Richards, J. L. et al. 2011, ApJS, 194, 29) which is supported in part by NASA grants NNX08AW31G, NNX11A043G, and NNX14AQ89G and NSF grants AST-0808050 and AST-1109911.

References

- Aartsen, M. G., Abbasi, R., Abdouand, Y., et al. 2013, *Science*, 342, 1242856
- Aartsen, M. G., Abraham, K., Ackermann, M., et al. 2015, *Astrophys. J.*, 809, 98
- Aartsen, M. G., Abraham, K., Ackermann, M., et al. 2017a, *Astrophys. J.*, 835, 151
- Aartsen, M. G., Abraham, K., Ackermann, M., et al. 2017b, *Astrophys. J.*, 835, 45
- Aartsen, M. G., Ackermann, M., Adams, J., et al. 2017a, *Journal of Instrumentation*, 12, P03012
- Aartsen, M. G., Ackermann, M., Adams, J., et al. 2017b, *Astroparticle Physics*, 92, 30
- Aartsen, M. G., Ackermann, M., Adams, J., et al. 2015, *ApJ*, 807, 46
- Aartsen, M. G., Ackermann, M., Adams, J., et al. 2018a, *Science*, 361, eaat1378
- Aartsen, M. G., Ackermann, M., Adams, J., et al. 2018b, *Science*, 361, 147
- Abeyssekara, A. U., Archer, A., Benbow, W., et al. 2018, *ApJ*, 861, L20
- Abolfathi, B., Aguado, D. S., Aguilar, G., et al. 2018, *ApJS*, 235, 42
- Acero, F., Ackermann, M., Ajello, M., et al. 2015, *ApJS*, 218, 23
- Ackermann, M., Ajello, M., Atwood, W. B., et al. 2015, *ApJ*, 810, 14
- Ackermann, M., Ajello, M., Atwood, W. B., et al. 2016, *ApJS*, 222, 5
- Ahlers, M. & Halzen, F. 2015, *Reports on Progress in Physics*, 78, 126901
- Ahn, C. P., Alexandroff, R., Allende Prieto, C., et al. 2012, *ApJS*, 203, 21
- Ajello, M., Atwood, W. B., Baldini, L., et al. 2017, *ApJS*, 232, 18
- Ajello, M., Romani, R. W., Gasparrini, D., et al. 2014, *ApJ*, 780, 73
- Alard, C. 2000, *A&AS*, 144, 363

¹⁹ Here we assume a signal fraction of our sample of 45 – 55%. The spread includes systematic uncertainties due to uncertainties in the assumed neutrino spectral shape and uncertainties in the signal fraction introduced by removing badly reconstructed events from the initial stream.

- Alard, C. & Lupton, R. H. 1998, *ApJ*, 503, 325
- Albert, A., André, M., Anghinolfi, M., et al. 2018, *ApJ*, 863, L30
- Ansoldi, S., Antonelli, L. A., Arcaro, C., et al. 2018, *ApJ*, 863, L10
- Atwood, W. B., Abdo, A. A., Ackermann, M., et al. 2009, *ApJ*, 697, 1071
- Bartos, I. & Kowalski, M. 2017, *Multimessenger Astronomy*, 2399-2891 (IOP Publishing)
- Bianchi, L., Shiao, B., & Thilker, D. 2017, *ApJS*, 230, 24
- Cerruti, M., Zech, A., Boisson, C., et al. 2019, *MNRAS*, 483, L12
- Drake, A. J., Djorgovski, S. G., Mahabal, A., et al. 2009, *ApJ*, 696, 870
- Evans, P. A., Osborne, J. P., Beardmore, A. P., et al. 2014, *ApJS*, 210, 8
- Gao, S., Fedynitch, A., Winter, W., & Pohl, M. 2018, *Nature Astronomy*, 154
- Gregory, P. C., Scott, W. K., Douglas, K., & Condon, J. J. 1996, *ApJS*, 103, 427
- Helfand, D. J., White, R. L., & Becker, R. H. 2015, *ApJ*, 801, 26
- Henden, A. A., Levine, S., Terrell, D., & Welch, D. L. 2015, in *American Astronomical Society Meeting Abstracts*, Vol. 225, American Astronomical Society Meeting Abstracts #225, 336.16
- IceCube Collaboration, Aartsen, M. G., Ackermann, M., et al. 2017, *ArXiv e-prints* [[arXiv:1710.01191](#)]
- Kadler, M., Krauß, F., Mannheim, K., et al. 2016, *Nature Physics*, 12, 807
- Keivani, A., Murase, K., Petropoulou, M., et al. 2018, *ApJ*, 864, 84
- Kochanek, C. S., Shappee, B. J., Stanek, K. Z., et al. 2017, *PASP*, 129, 104502
- Krauß, F., Wilms, J., Kadler, M., et al. 2016, *A&A*, 591, A130
- Laher, R. R., Surace, J., Grillmair, C. J., et al. 2014, *PASP*, 126, 674
- Lambert, S. B. & Gontier, A. M. 2009, *A&A*, 493, 317
- Liu, R.-Y., Wang, K., Xue, R., et al. 2018, *ArXiv e-prints* [[arXiv:1807.05113](#)]
- Lott, B., Escande, L., Larsson, S., & Ballet, J. 2012, *A&A*, 544, A6
- Lucarelli, F., Tavani, M., Piano, G., et al. 2019, *ApJ*, 870, 136
- Mannheim, K. 1995, *Astroparticle Physics*, 3, 295
- Masci, F. J., Laher, R. R., Rebbapragada, U. D., et al. 2017, *PASP*, 129, 014002
- Maselli, A., Massaro, F., D'Abrusco, R., et al. 2015, *Astrophys. Space Sci.*, 357, 141
- Massaro, E., Perri, M., Giommi, P., & Nesci, R. 2004, *Astron. Astrophys.*, 413, 489
- Murase, K. 2015, *ArXiv e-prints* [[arXiv:1511.01590](#)]
- Murase, K., Guetta, D., & Ahlers, M. 2016, *Physical Review Letters*, 116, 071101
- Murase, K., Oikonomou, F., & Petropoulou, M. 2018, *ApJ*, 865, 124
- Padovani, P., Giommi, P., Resconi, E., et al. 2018, *MNRAS*, 480, 192
- Padovani, P. & Resconi, E. 2014, *MNRAS*, 443, 474
- Padovani, P., Resconi, E., Giommi, P., Arsioli, B., & Chang, Y. L. 2016, *MNRAS*, 457, 3582
- Paiano, S., Falomo, R., Treves, A., & Scarpa, R. 2018, *ApJ*, 854, L32
- Reimer, A. et al. 2018, in *prep.*
- Rosen, S. R., Webb, N. A., Watson, M. G., et al. 2016, *A&A*, 590, A1
- Scargle, J. D., Norris, J. P., Jackson, B., & Chiang, J. 2013, *ApJ*, 764, 167
- Shappee, B. J., Prieto, J. L., Grupe, D., et al. 2014, *ApJ*, 788, 48
- Snellen, I. A. G., McMahon, R. G., Hook, I. M., & Browne, I. W. A. 2002, *MNRAS*, 329, 700
- Stecker, F. W. 2013, *Phys. Rev. D*, 88, 047301
- Stecker, F. W., Done, C., Salamon, M. H., & Sommers, P. 1991, *Physical Review Letters*, 66, 2697
- Strotjohann, N. L., Kowalski, M., & Franckowiak, A. 2018 [[arXiv:1809.06865](#)]
- Tanaka, Y. T., Buson, S., & Kocevski, D. 2017, *The Astronomer's Telegram*, 10791
- Tavecchio, F. & Ghisellini, G. 2015, *MNRAS*, 451, 1502
- Wright, E. L., Eisenhardt, P. R. M., Mainzer, A. K., et al. 2010, *AJ*, 140, 1868
- Zhang, H., Fang, K., & Li, H. 2018, *ArXiv e-prints* [[arXiv:1807.11069](#)]
- III. Physikalisches Institut, RWTH Aachen University, D-52056 Aachen, Germany
- ² Department of Physics, University of Adelaide, Adelaide, 5005, Australia
- ³ Dept. of Physics and Astronomy, University of Alaska Anchorage, 3211 Providence Dr., Anchorage, AK 99508, USA
- ⁴ Dept. of Physics, University of Texas at Arlington, 502 Yates St., Science Hall Rm 108, Box 19059, Arlington, TX 76019, USA
- ⁵ CTSPS, Clark-Atlanta University, Atlanta, GA 30314, USA
- ⁶ School of Physics and Center for Relativistic Astrophysics, Georgia Institute of Technology, Atlanta, GA 30332, USA
- ⁷ Dept. of Physics, Southern University, Baton Rouge, LA 70813, USA
- ⁸ Kavli Institute for Astronomy and Astrophysics, Peking University, 5 Yiheyuanlu, Haidian District Beijing, China 100871
- ⁹ Dept. of Physics, University of California, Berkeley, CA 94720, USA
- ¹⁰ Lawrence Berkeley National Laboratory, Berkeley, CA 94720, USA
- ¹¹ Institut für Physik, Humboldt-Universität zu Berlin, D-12489 Berlin, Germany
- ¹² Fakultät für Physik & Astronomie, Ruhr-Universität Bochum, D-44780 Bochum, Germany
- ¹³ Université Libre de Bruxelles, Science Faculty CP230, B-1050 Brussels, Belgium
- ¹⁴ Vrije Universiteit Brussel (VUB), Dienst ELEM, B-1050 Brussels, Belgium
- ¹⁵ Dept. of Physics, Massachusetts Institute of Technology, Cambridge, MA 02139, USA
- ¹⁶ Dept. of Physics and Institute for Global Prominent Research, Chiba University, Chiba 263-8522, Japan
- ¹⁷ Dept. of Physics and Astronomy, University of Canterbury, Private Bag 4800, Christchurch, New Zealand
- ¹⁸ Dept. of Physics, University of Maryland, College Park, MD 20742, USA
- ¹⁹ Dept. of Astronomy, Ohio State University, Columbus, OH 43210, USA
- ²⁰ Dept. of Physics and Center for Cosmology and Astro-Particle Physics, Ohio State University, Columbus, OH 43210, USA
- ²¹ Center for Cosmology and Astroparticle Physics, The Ohio State University, Columbus, OH 43210, USA
- ²² Niels Bohr Institute, University of Copenhagen, DK-2100 Copenhagen, Denmark
- ²³ Dept. of Physics, TU Dortmund University, D-44221 Dortmund, Germany
- ²⁴ Dept. of Physics and Astronomy, Michigan State University, East Lansing, MI 48824, USA
- ²⁵ Dept. of Physics, University of Alberta, Edmonton, Alberta, Canada T6G 2E1
- ²⁶ Erlangen Centre for Astroparticle Physics, Friedrich-Alexander-Universität Erlangen-Nürnberg, D-91058 Erlangen, Germany
- ²⁷ Physik-department, Technische Universität München, D-85748 Garching, Germany
- ²⁸ Département de physique nucléaire et corpusculaire, Université de Genève, CH-1211 Genève, Switzerland
- ²⁹ Dept. of Physics and Astronomy, University of Gent, B-9000 Gent, Belgium
- ³⁰ Institute for Astronomy, University of Hawai'i, Honolulu, HI 96822, USA
- ³¹ Dept. of Physics and Astronomy, University of California, Irvine, CA 92697, USA
- ³² Dept. of Physics and Astronomy, University of Kansas, Lawrence, KS 66045, USA
- ³³ SNOLAB, 1039 Regional Road 24, Creighton Mine 9, Lively, ON, Canada P3Y 1N2
- ³⁴ Department of Physics and Astronomy, UCLA, Los Angeles, CA 90095, USA
- ³⁵ Dept. of Astronomy, University of Wisconsin, Madison, WI 53706, USA
- ³⁶ Dept. of Physics and Wisconsin IceCube Particle Astrophysics Center, University of Wisconsin, Madison, WI 53706, USA
- ³⁷ Institute of Physics, University of Mainz, Staudinger Weg 7, D-55099 Mainz, Germany
- ³⁸ Department of Physics, Marquette University, Milwaukee, WI, 53201, USA

- ³⁹ Institut für Kernphysik, Westfälische Wilhelms-Universität Münster, D-48149 Münster, Germany
- ⁴⁰ Bartol Research Institute and Dept. of Physics and Astronomy, University of Delaware, Newark, DE 19716, USA
- ⁴¹ Dept. of Physics, Yale University, New Haven, CT 06520, USA
- ⁴² Dept. of Physics, University of Oxford, Parks Road, Oxford OX1 3PQ, UK
- ⁴³ Dept. of Physics, Drexel University, 3141 Chestnut Street, Philadelphia, PA 19104, USA
- ⁴⁴ Physics Department, South Dakota School of Mines and Technology, Rapid City, SD 57701, USA
- ⁴⁵ Dept. of Physics, University of Wisconsin, River Falls, WI 54022, USA
- ⁴⁶ Dept. of Physics and Astronomy, University of Rochester, Rochester, NY 14627, USA
- ⁴⁷ The Observatories of the Carnegie Institution for Science, 813 Santa Barbara St., Pasadena, CA 91101, USA
- ⁴⁸ Núcleo de Astronomía de la Facultad de Ingeniería y Ciencias, Universidad Diego Portales, Av. Ejército 441, Santiago, Chile
- ⁴⁹ Millennium Institute of Astrophysics, Santiago, Chile
- ⁵⁰ Oskar Klein Centre and Dept. of Physics, Stockholm University, SE-10691 Stockholm, Sweden
- ⁵¹ Dept. of Physics and Astronomy, Stony Brook University, Stony Brook, NY 11794-3800, USA
- ⁵² Dept. of Physics, Sungkyunkwan University, Suwon 16419, Korea
- ⁵³ Dept. of Physics and Astronomy, University of Alabama, Tuscaloosa, AL 35487, USA
- ⁵⁴ Dept. of Astronomy and Astrophysics, Pennsylvania State University, University Park, PA 16802, USA
- ⁵⁵ Dept. of Physics, Pennsylvania State University, University Park, PA 16802, USA
- ⁵⁶ Dept. of Physics and Astronomy, Uppsala University, Box 516, S-75120 Uppsala, Sweden
- ⁵⁷ NASA Postdoctoral Program Fellow, Universities Space Research Association, USA
- ⁵⁸ now at University of Würzburg, 97074 Würzburg, Germany
- ⁵⁹ University of Maryland, Baltimore County, MD, USA
- ⁶⁰ Dept. of Physics, University of Wuppertal, D-42119 Wuppertal, Germany
- ⁶¹ DESY, D-15738 Zeuthen, Germany
- ⁶² Earthquake Research Institute, University of Tokyo, Bunkyo, Tokyo 113-0032, Japan